# TRAVELING-WAVE CHARGED PARTICLE GENERATION

Author: Lance Herold

Thesis Supervisor:
Professor J.R. Melcher

Date Submitted: May 19, 1967

# TRAVELING-WAVE CHARGED PARTICLE GENERATION

by

LANCE HEROLD

BS UNITED STATES NAVAL ACADEMY

(1958)

SUBMITTED TO THE DEPARTMENT OF NAVAL ARCHITECTURE AND MARINE ENGINEERING IN PARTIAL FULFILLMENT OF THE REQUIREMENTS OF THE MASTER OF SCIENCE DEGREE IN ELECTRICAL ENGINEERING AND THE PROFESSIONAL DEGREE, NAVAL ENGINEER

at the

MASSACHUSETTS INSTITUTE OF TECHNOLOGY

May, 1967

Signature of Author. . . . . .
Department of Naval Architecture and Marine Engineering, May 19, 1967.

Certified by . . . . . .
Thesis Supervisor

Certified by. . . . . .
Reader for the Department

Accepted by. . . . . .
Chairman, Departmental Committee on Graduate Students

# TRAVELING-WAVE CHARGED PARTICLE GENERATION

by

LANCE HEROLD

## ABSTRACT

Submitted to the Department of Naval Architecture and Marine Engineering on May 19, 1967 in partial fulfillment of the requirements for the Master of Science Degree in Electrical Engineering and the Professional Degree, Naval Engineer.

A sinusoidally charged aerosol is injected into a fluid flow and interacts synchronously with a traveling wave of voltage. The voltage traveling wave can either be that induced on passively loaded channel electrodes, or externally supplied and adjusted to either lead or lag the charge wave. In both the passive loading and lagging impressed-voltage cases, fluid dynamic to electrical energy conversion is achieved, while in the case of voltage wave leading the charge wave , electrical pumping of the fluid flow occurs. This study concentrates on an induction method of charging a distilled water aerosol formed in a set of spray atomization nozzles using compressed air.

Historical background of direct-current electro-fluid dynamic energy conversion is outlined, along with a theoretical comparison with what is considered a hitherto untried synchronous approach to the problem.

Experiments were conducted to determine a feasible method of inducing alternating charge on aerosol droplets; small enough to produce useful concentrations, and large enough for substantial viscous coupling with the transport medium. The resulting charged aerosol generator is described and analyzed.

Thesis Supervisor: James R. Melcher
Title: Associate Professor of Electrical Engineering

## LIST OF FIGURES

## LIST OF SYMBOLS

$a$ . . . . . Droplet radius

$E$ . . . . . Electric field

$E_b$ . . . . . Breakdown field strength ( $3 \times 10^4$ v/cm in air)

EFD . . . . . Electro-Fluid Dynamic

$e$ . . . . . charge of one electron ($1.602 \cdot 10^{-19}$ coul)

$I_o$ . . . . . Output current from generator

$(\bar{i}_k)$ . . . . . Unit vector in the k-direction

$J$ . . . . . Current density (amp/$m^2$)

$K$ . . . . . Mobility

$P$ . . . . . Power

$p$ . . . . . Pressure

$Q$ . . . . . Flow rate (gal/hr. or $cm^3$/sec)

$q$ . . . . . Charge per droplet

$u$ . . . . . Drift velocity

$U_o$ . . . . . Velocity of transport medium

$V_o$ . . . . . Maximum value of voltage on channel electrode

$\mu$ . . . . . Coefficient of Viscosity ($184 \cdot 10^{-6}$ gm/sec·cm for air) at $20^\circ$ C

$\varepsilon$ . . . . . General electrical permitivity

$\varepsilon_o$ . . . . . Electrical permitivity of air
($8.85 \times 10^{-12}$ coul$^2$/newt$\cdot$m$^2$)

$\sigma$ . . . . . Surface charge density
(coul/m$^2$)

$\rho$ . . . . . Volumetric charge density
(coul/m$^3$)

$\rho_m$ . . . . . Mass density
(Kg/m$^3$ or gm/cm$^3$)

$\mu$a . . . . . Micro amperes
($10^{-6}$ amps)

$\mu$m . . . . . Micron
($10^{-4}$ cm)

$\gamma$ . . . . . Surface tension
(73.05 dyne/cm for water)

$\hat{(\ )}$ . . . . . Quantity ( ) is complex

$\hat{(\ )}^*$ . . . . . Complex conjugate of quantity ( )

$\overline{(\ )}$ . . . . . ( ) is spacial vector

$\langle\ \rangle$ . . . . . time average

$|\ |$ . . . . . Magnitude of included quantity

f . . . . . Frequency
(cycles/sec)

$\omega$ . . . . . Frequency
(radius/sec)

## ACKNOWLEDGEMENTS

The author expresses appreciation to Professor J.R. Melcher, who developed the synchronous EFD energy conversion theory, for his active interest and support. Among the other members of the Continuum Electromechanics Group who contributed helpful suggestions and material assistance are Harold Atlas and Edward Devitt, for their aid in obtaining material and construction of apparatus, and William Reeve, who was co-participant in the over-all project.

Indebtedness is also acknowledged to A.J. McElroy and Craig Kirkwood for their assistance in generating, collecting, and photographing the aerosol droplets.

Financial support for this research was provided by the National Aeronautics and Space Administration and the United States Navy.

TABLE OF CONTENTS

# I. INTRODUCTION

## A. Background

Mechanical to electrical energy conversion systems have traditionally employed the interaction of charge in motion and magnetic fields. Since magnetic field energy densities are characteristically orders of magnitude greater than those of electric fields, relatively little attention has been directed toward electric field energy conversion machines.

A characteristic of Electro-Fluid Dynamic systems in general, has been their high voltages (tens of kilovolts) and small currents (microamp to milliamp regime). Electrostatic effects are often observed in corona discharge from long wires during snow storms, lightning, and other natural phenomena which seem to have inspired some of the early work in electric field energy conversion. The earliest converters were Van de Graaff - type systems, in that they employed frictional or corona electrification and mechanical transport of the charged particles to a region of high potential. One of the first EFD generators was proposed by R.E. Vollrath[1] in 1932. His was a high voltage generator using blown powder, contact electrified, and carried to a metal sphere at high electric potential. This model was more in line with present work, since it involved gas dynamic propulsion of the charges.

The literature contains few, if any, significant developments in the field from 1932 until the early 1950 s. In 1953,

A.M. Marks[7] obtained a patent for a thermo-electric power converter using a charged aerosol. Others had begun taking at least a limited second look at EFD machines as a possible method of producing electrical power without mechanical complexity, and hopefully, at higher power to weight ratios than are obtainable with magnetohydrodynamic systems.

Within the last decade there has been a burst of activity in the study of electro-fluid dynamic energy conversion processes. The impetus for such research has come largely from the need for simple, light weight and reliable generators to be carried in space vehicles. An EFD-type system would uniquely meet these particular requirements if sufficient power levels and electrical efficiencies could be achieved. To this end, a number of feasibility studies have been conducted and various types of experimental systems have been constructed. It should be noted that all published work, to date, seems to have been limited to uni-polar (d-c) EFD systems.

## B. Feasibility Considerations

### 1. Mobility

The most basic limitation on EFD energy converters is their extremely low efficiency in terms of electrical energy output for fluid dynamic energy input. A major reason for this is the limited nature of the interaction mechanism between charge carriers and the transporting medium. This has historically been expressed as mobility (K), defined as the

ratio of drift velocity to the electric field.

$$K = \frac{u}{E} \tag{I.1}$$

Since the electric force on a charge carrying particle is the charge multiplied by the electric field,

$$F = qE \tag{I.2}$$

the mobility can be expressed as:

$$K = \frac{uq}{F} \tag{I.3}$$

The nature of mobility for various fluid working media and particle sizes is described in several of the references and summarized in Appendix A. The facts which emerge from mobility consideration are that energy conversion efficiency increases as mobility decreases, and that the best coupling forces are achieved when the particles are large enough to obtain viscous interaction. The latter has been found to require particle sizes greater than about 1 micron diameter[7, 15].

Using Stokes' law, the force balance equation for a particle becomes:

$$F = qE = 6\pi u a \mu \tag{I.4}$$

Combining equations (I.3) and (I.4):

$$K = \frac{q}{6 \pi \mu a} \qquad (I.5)$$

The fact that mobility varies inversely with viscosity led to some experimentation with non-conducting liquids. In 1961, Stuetzer[3] presented the results of theoretical and experimental work with a small high voltage generator using transformer oil, kerosene, and air as the working media, and ions as charge carriers.

The use of liquid transport media has two disadvantages which seem to have limited its consideration, especially for space vehicle generators or propulsion systems. These are the extra added weight and the increased wall friction losses.

There are, in general, two ways of minimizing the effects of mobility in a gaseous medium.

(1) Increasing operating pressure and flow velocity to decrease mobility (see Appendix A), and make drift velocities negligible with respect to the flow velocity.

(2) Increase droplet size (at constant charge per droplet) to reduce mobility in accordance with Stokes' law.

In the case where ions are the charge carriers, method (1)

is usually applied [8, 11, 15]. A combination of the two methods is contained in the device described by Marks, Barreto, and Chu in Reference 7. As might be expected, however, factors which decrease mobility often have an adverse effect on other parameters of the system.

2. The Ballistic Approach

Mobility can be reduced or removed entirely as a factor in system performance by converting only the kinetic energy of the charge carriers into electrical energy. This is accomplished by injecting colloidal or ionic charged particles, at high velocity, into a very low pressure converter where viscous effects would be minimized.

Hasinger[18] gives a detailed theoretical analysis of this "Ballistic" type system, where he represents the energy conversion by equating the electrical power output to the change in kinetic energy between inlet and exit electrodes.

$$qV = \frac{1}{2} m (v_1^2 - v_2^2) \qquad (I.6)$$

where: $V$ = electrical potential between inlet and outlet

He also points out that an inherent loss comes from the necessity of allowing sufficient exit velocity to overcome space charge effects at the electrode, and variations in particle sizes. Hasinger concluded that 25 per cent of the kinetic energy should remain at the collector to meet these

considerations. Accordingly, $v_2$ will be half of $v_1$.

By considering space charge density in the conversion section to produce an electric field exactly offsetting that of the collector, Hasinger arrives at a simple expression for the upper limit on the electric force concentration in the ballistic generator.

$$\text{Force/unit area} = \frac{\varepsilon}{2} E_1^2 \qquad \text{(I.7)}$$

where: $E_1$ is the field at the entrance electrode, acting to decelerate the charged particles

With the 25 percent loss, this leads to an expression for power concentration

$$\text{Power/unit area} = \frac{3}{8} E_1^2 U_o \qquad \text{(I.8)}$$

for which Hasinger concludes that concentration of 300 watts/cm$^2$ should be feasible.

A type of ballistic EFD generator is described in Reference 6 and further discussed in Reference 8. Disadvantages characteristic of ballistic systems are the requirement for focusing the particle beam, and difficulties inherent in the basic concept for recirculation or successive staging in a closed, low pressure system.

3. Viscous-Coupled System Performance

The basic theoretical performance capability of an EFD system is derived in Appendix A.3 following the simplified model used by Lawson [13]. The resulting expression for the maximum power per unit area which can ideally be extracted from the flow, in the form of pressure drop times velocity, is

$$\Delta p \cdot U_o = \frac{\varepsilon_o}{2} E_b^2 \cdot U_o \qquad (I.9)$$

This result is not surprising, but indicates the nature of the problem which presents itself when one contemplates the extraction of significant electrical energy from fluid dynamic head. As Lawson observes, when the parameter values corresponding to atmospheric pressure are inserted into equation (I.9), the maximum pressure drop is about $4 \times 10^{-4}$ atmospheres. By increasing the pressure to 30 atmospheres the maximum $\Delta p$ increases to about one third of the standard atmosphere. This type of analysis seems to indicate, therefore, that in order for such a system to attain practicability, some kind of multi-staging in a closed system would be required.

The concept of multi-staging imposes additional limitations on system performance. Since frictional power losses are proportional to $(U_o)^3$, each collector grid and attractor electrode added to the channel further restricts the allowable flow velocity.

Recognizing this, Lawson defines stage efficiency as

$$\eta_{st} = \frac{L_e}{L_f + L_d} \tag{I.10}$$

where: $L_e$ is electrical power density (see equation (A.28))

$L_f$ is fluid power input (I.9)

$L_d$ is fluid dynamic power loss

$$L_d = \alpha \rho_m \frac{U_o^3}{2} \tag{I.11}$$

where: $\alpha$ is a constant coefficient appropriate for the particular electrode and channel wall configuration.

The expression for the maximum attainable stage efficiency is then,

$$\eta_{st} = \frac{\frac{\varepsilon_o}{2} E_b^2 (U_o - K E_b)}{\frac{\varepsilon_o}{2} E_b^2 U_o + \alpha \rho_m \frac{U_o^3}{2}}$$

or

$$\eta_{st} = \frac{1 - \frac{K E_b}{U_o}}{1 + \frac{\alpha \rho_m U_o^2}{\varepsilon_o E_b^2}} \tag{I.12}$$

Using air at 30 atmospheres pressure as the working medium, with flow speed of 50 m./sec., and colloids as charge carriers for negligible mobility, Lawson arrives at a representative stage efficiency of 80 percent with a power concentration of 200 watts/$cm^2$.

It must be emphasized that this is a theoretical limit, does not consider exit velocity as a loss, and that present state of the art is a long way from physical realization of this performance.

## C. PROPOSED SYSTEM

Operation of an EFD energy conversion system for "alternating current" charged particles has been virtually ignored. Von Ohain and Wattendorf recommend such research[12], but apparently only within the context of the system described in the previous section. That is, the same transport and collection mechanisms would be employed.

The synchronous EFD system investigated and described in this report, and in Reference 19, is based on an induction concept which is believed to be unique in this application, and possessed of distinct advantages over existing systems.

### 1. Description

Sinusoidally charged droplets are injected into a fluid dynamic flow to create a traveling wave of charge confined in a channel. Electrodes are suitably placed along the

channel walls to interact synchronously with the charge wave; either to convert fluid dynamic to electrical energy, or vice-versa, in which case the system acts as a pump.

There are basically three "modes" of operation for such a system.

1. Channel electrodes are passively loaded (R,L,C)
2. A traveling wave of voltage is impressed on the electrodes which "leads" the wave of charge
3. The impressed voltage wave "lags" the wave of charge.

The basic theory of the energy conversion mechanism is derived in Appendix A and discussed in greater detail in Reference 19. The form of the solution (equation A.19, page 48) suggests the analogy between this synchronous EFD system and the magnetic field/torque angle relationships which obtain in conventional rotating machinery systems.

In this regard, modes (1) and (2) correspond to a synchronous motor, while mode (3) corresponds to a synchronous generator. The channel electrodes are analogous to the stator and the fluid flow corresponds to the rotor.

## 2. Advantages of Synchronous System

The fundamental reason for interest in alternating current EFD power generation is the possibility it offers for obtaining a-c power in a system requiring neither moving parts nor electronic conversion of d-c. In addition to the

previously mentioned advantages of the direct EFD systems, the synchronous generator concept inherently resolves several of the major difficulties.

Because the charges need not be collected in order to produce electrical power, the channel can be kept free of obstructions downstream from the charge wave source, and the system frictional losses are produced by wall friction alone. Multi-staging is a built-in feature of the concept, since each wave length of electrodes is equivalent to a stage.

The principal restriction on flow velocity comes from the relationship between velocity, frequency, and wave length in a traveling wave. Thus, at a given frequency, the length of channel per stage is proportional to $U_o$.

The flexibility of this system, in its capability for pumping non-conducting fluids as well as for electrical power generation, may eventually prove to be a significant advantage.

Another restriction on synchronous system performance comes from lateral stress on the charge flow due to the wall electrodes. This is in addition to the space charge forces existent in the d-c converter, and may prove to be a restriction on the number of wave lengths which can be accommodated between renewals of the charge wave.

The intention of this thesis research was to experimentally test the conversion mechanism theoretically predicted, and to investigate an induction method of generating the charged droplet wave.

## II. EXPERIMENTAL PROCEDURE

### A. Description of Initial Experiments

Initial experimentation was conducted using droplets issuing from capillary tubes placed directly in the air stream from the axial fan. At this stage the objective was to use the maximum droplet size which did not result in wetting of the channel walls and consequent shorting of the output electrodes.

Various means of introducing the water droplets and various inducer electrode configurations were investigated. These included from one to five - 10 mil inside diameter capillary tubes mounted in a 1/8 inch O.D. tube which was inserted either from the side of the channel or from the narrow ends. Because of turbulence created in the channel, the latter method proved more satisfactory from the standpoint of channel wetting. For these experiments the excitation was provided by a 2 to 5 kilovolt, 60-cycle signal applied to a pair of wires in mid-channel, running vertically one centimeter apart, and about .6 cm. from the ends of the tubes. The experimental apparatus is shown in Figure 1.

The droplets were drawn out of the capillary tubes by a combination of hydrostatic head, eductor action of the air stream, and electrostatic stress as described in Appendix

B. Of these, the hydrostatic head was by far the major factor, and variations in output current were observed to conform to the rate of droplet formation due to variations in water pressure. It was also readily apparent that the maximum charge per droplet was at least an order of magnitude less than Rayleigh's limit and imposed no restriction on the results.

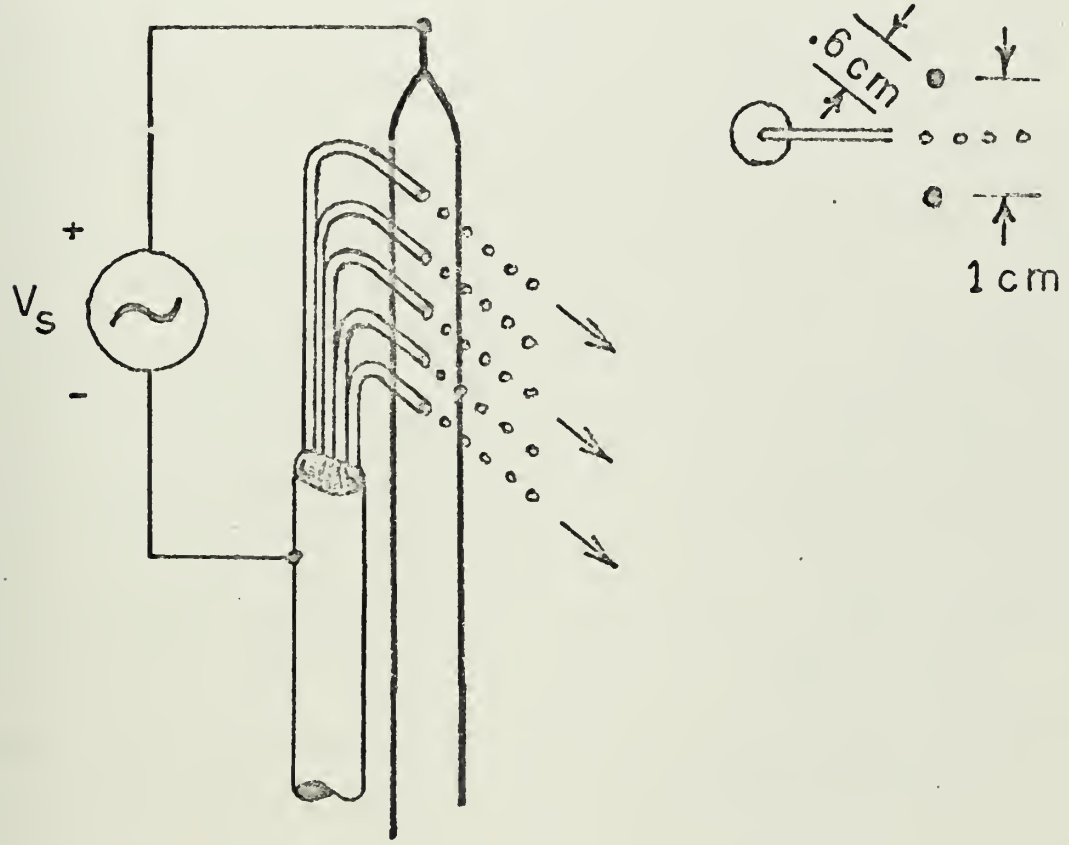


Figure 1. CAPILLARY TUBE AND INDUCER APPARATUS
For LARGE droplets

The droplets were collected at the end of the channel by a wire mesh suspended from insulators within a shielded box and discharging through an impedance of .65 megohms. Crude as the instrumentation proved to be, the quality of the measured signal could be observedly improved by increasing the number of droplets, since the rate of emission of droplets must clearly be greater than 60 per second if a relatively smooth 60 cycle current is to be produced.

With droplets as large as those emerging from the smallest capillary tubes, any contact with the channel walls is unacceptable. This aspect of the problem proved to be such a dominant constraint that it dictated all subsequent designs.

As an illustration of the effect of turbulence, a 28 mil O.D. capillary tube was mounted in the end of a one eighth inch feed tube which was then inserted into the 60 feet per second air flow, just downstream of the flow straightener section in the 2 1/4 inch by 6 inch channel. The feed tube entered from the middle of the 6 inch, "near" side of the channel. With the mouth of the capillary tube positioned at mid-channel there was no wetting of either side in the 36 inch downstream electrode section. The turbulence at the near wall prevented the droplets from being positioned more than about 1/8 inch off-center in that direction without wetting in the channel. The absence of additional turbulence at the far wall permitted movement of the droplet emitter to within about 3/8 inch of that side before the onset of wetting

down channel.

Because of this limitation on the distribution of large droplets no further work with them was attempted in the course of this particular project. This is not to say that such a study would necessarily be impractical, however, and further commentary on this subject is made in the recommendations of Chapter VI.

## B. Small Droplet Experiments

### Considerations

As described in section C of Chapter I, mobilities deriving from the application of Stokes' law are achieved as long as droplet diameters are on the order of one micron or greater. Since a complete investigation of system performance using the entire range of droplet sizes was not feasible for this study, it was decided to concentrate on the production of charged "fog" droplets; approximately 1 to 20 microns in diameter. The objective was to fill the channel with droplets large enough to obtain satisfactory viscous coupling with the air stream, but small enough to permit evaporation to offset the deposition of droplets on the plexiglass wall surfaces.

Another advantage of using fog droplets comes from the signal smoothing effect of a high rate of charge carrier

formation. An obvious disadvantage is the greater difficulty of inducing alternating charge on aerosol sprayed droplets. Learning the extent of this problem and the possibilities of solving it became the next experimental objective.

Spray Nozzle Experiments

A commercial type spray nozzle was used for feasibility investigation. The particular configuration for air and water mixing is shown in Figure 2. It was assumed that this method of fog generation would provide the best type of water jet break up from the standpoint of accessibility to the inducing field.

Nozzles which mix air and water before emission could be expected to be less desirable because of the poor conductivity of the fog, even at the initial concentration. Another method of aerosol generation consists of intersecting air and water jets, but it was not tried for this narrow channel because of the better directional control afforded by a nozzle.

The other advantageous feature of the concentric air jet is the shield it provides around the water stream. This enables the inducer electrode to be positioned close to the region of the fog formation with minimum possibility of an electrical short circuit between electrode and water. This was tested by mounting the commercial nozzle in a piece of plexiglass with a circular inducing electrode of 3/16 inch diameter centered on the nozzle outside of a 1/16 inch

plexiglass separation.

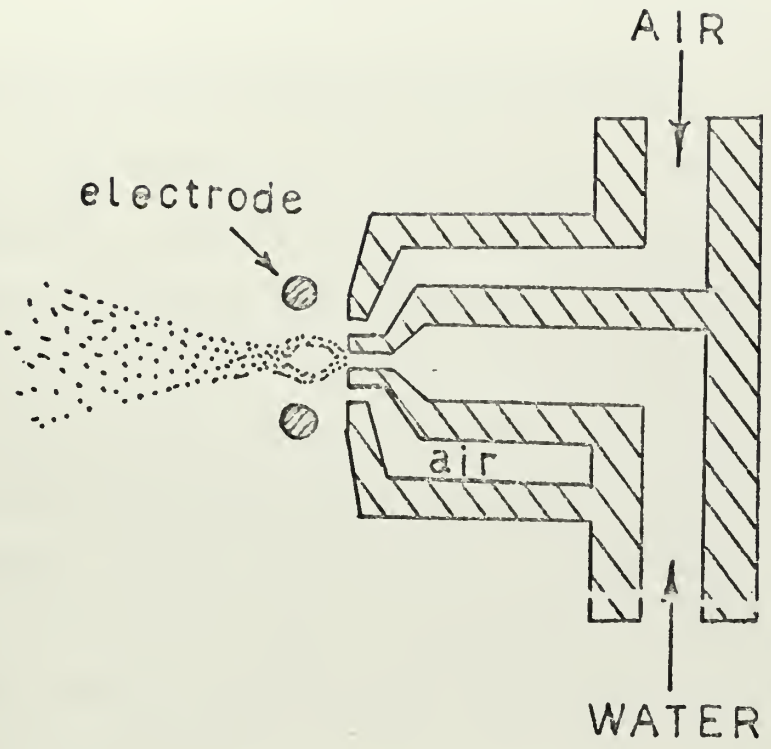


Figure 2. COMMERCIAL NOZZLE SCHEMATIC

Experiments did show, that significant charge can be induced on the fog droplets in this way.

The results of the experiments with the commercial nozzle are plotted in the next chapter in Figure 3. The current produced by this configuration was about 2 orders of magnitude greater than that produced by the capillary tube experiments. It should be noted that the measurements of Figure 3 were made with the nozzle outside of the channel and are the total

current produced by one nozzle. A rough drawing of this nozzle and electrode is presented in Figure 10.

Nozzle Design for the Charge Wave Generator

Having established the feasibility of using aerosol spray technique, the next step was to achieve a design which could fill the channel with droplets with minimum interference with the air stream and wetting of the channel walls. Catalog information for the commercial nozzle describes the qualitative effect of variations in the air pressure with respect to flow rate and average droplet size. The effect of increasing air flow, at constant water siphon height, is to retain or slightly decrease the droplet diameter while increasing the water flow rate.

Several different nozzle designs were constructed using capillary tubes of varying diameter together with various sized air annuli. The process leading to the result shown in Figure 16 was largely trial and error, first using steel and plastic tubing, and finally plexiglass and stainless steel capillary tubes.

Two different sets of plexiglass and capillary tube nozzles finally resulted. The first consisted of five vertically aligned nozzles in each of two 3/16 inch thickness plexiglass sections. These used 10 mil inside diameter capillary tubes and were designed to produce a fine spray

on the order of a few microns diameter. The second was similar, but contained 10 nozzles in each bank and used 15 mil inside diameter tubes to produce a great quantity of larger droplets, on the order of 20 microns diameter.

Another feature which distinguished the two designs was the inducing electrode configuration. The fine droplet design used a flush, painted electrode surrounding the air ring, while the other consisted of 72 mil O.D. tubing sections, of about 2 mm length, concentric to the nozzle aperture.

A detailed description of the nozzle and electrode designs, with diagrams of the apparatus, is contained in Appendix B.2. Photographs of the generator apparatus, 20-nozzle unit, and generated aerosol, are included in the next chapter.

# III. RESULTS

## A. General Description

The charged aerosol generator units which finally evolved in the course of experimentation were successful in producing a significant charge wave of droplets of the desired size. In addition, the input impedance is infinite as frequency goes to zero, consisting of "pure" capacitance, as was desired.

In order to evaluate the generator design it was necessary to make a number of measurements of the system parameters. Because the nozzles and electrodes were handmade it was difficult to get completely consistent measurements from day to day. Non-uniformities such as capillary tubes being slightly off-center in the air jets and electrodes, variations in the pressure from the air supply, and inherent difficulties in measuring small currents in an aerosol spray over a range of flow conditions, were some of the contributing factors. The data summarized in Appendix D is, for the most part, the result of 4 or 5 reasonably consistent test series. Since the objective of the project was primarily exploratory in nature; to investigate feasibility of the general concept, sophisticated instrumentation was not employed, or considered a productive goal at this stage of system development.

Photographs of the apparatus and generated aerosol are displayed in Figure 5.

B. Graphical Summary of Results

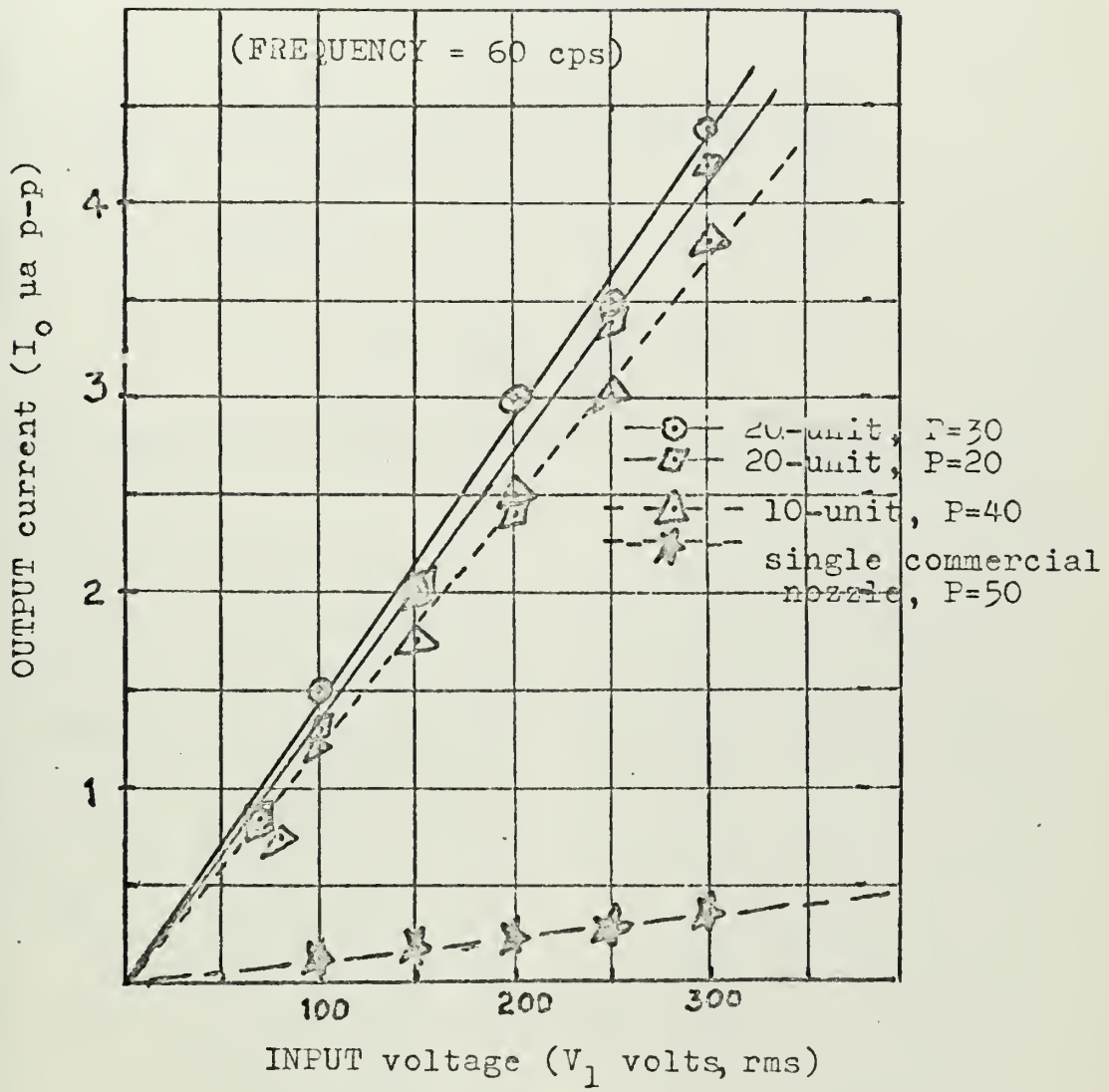


Figure 3.

OUTPUT CURRENT VS. INPUT VOLTAGE

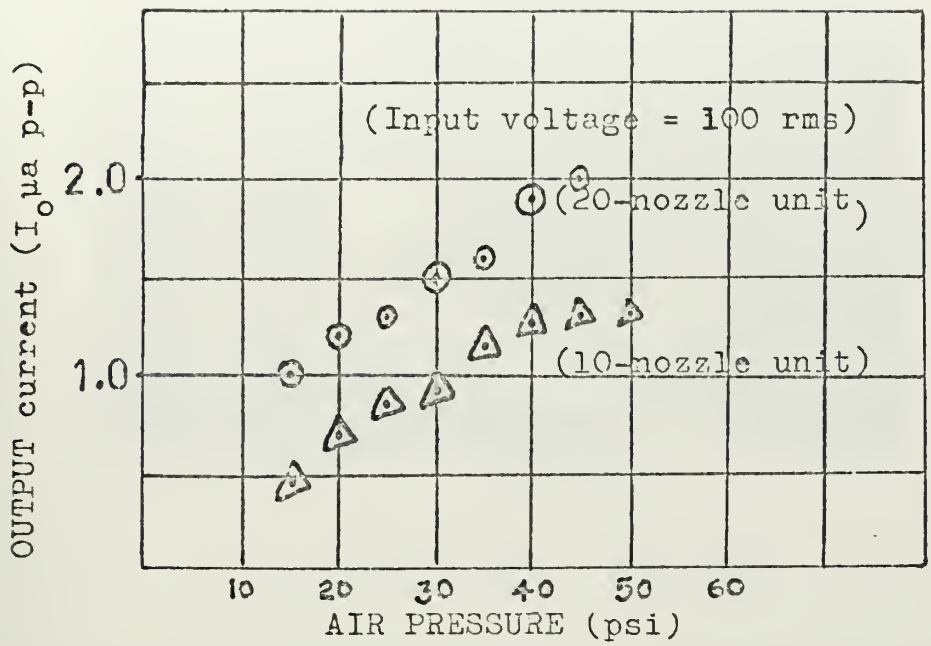


Figure 4a. OUTPUT CURRENT VS. AIR PRESSURE

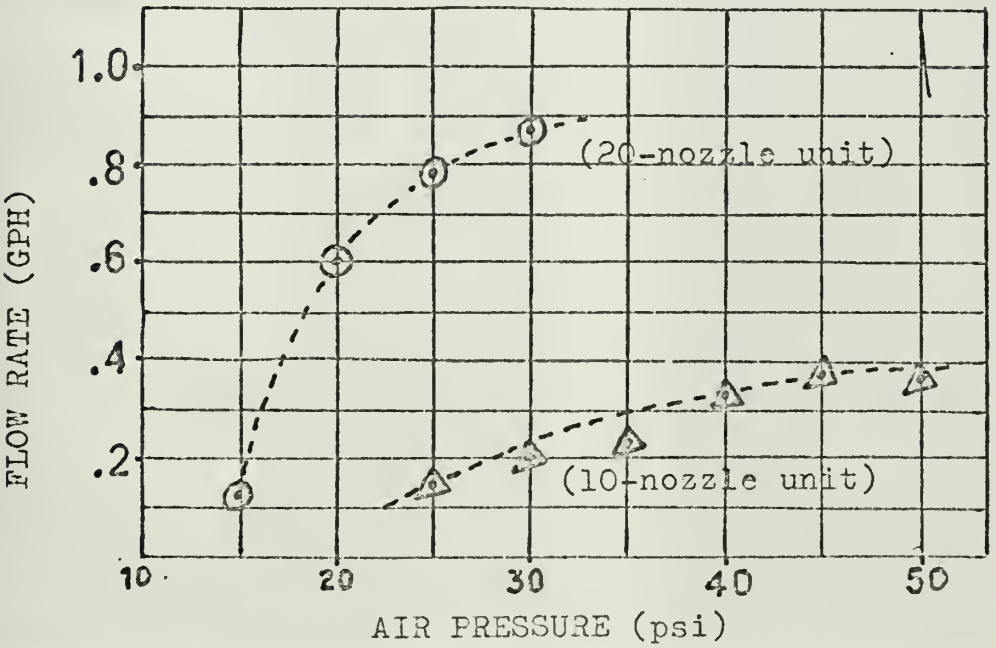


Figure 4b. WATER FLOW RATE VS. AIR PRESSURE

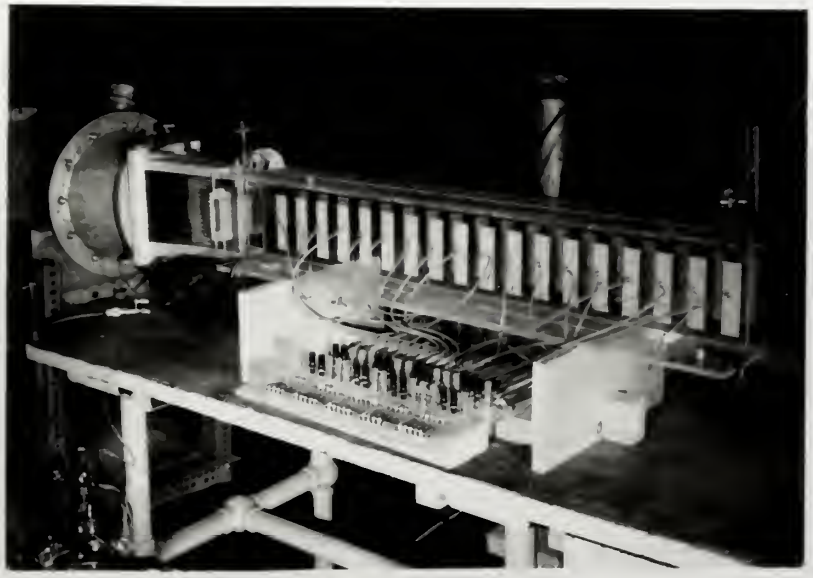

SYNCHRONOUS GENERATOR APPARATUS

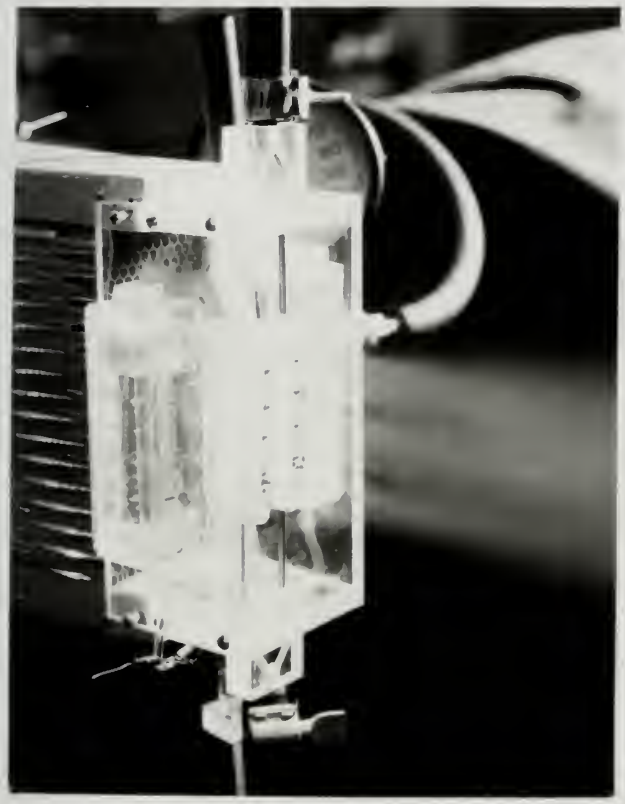

CHARGED AEROSOL Generated
by 10-nozzle unit

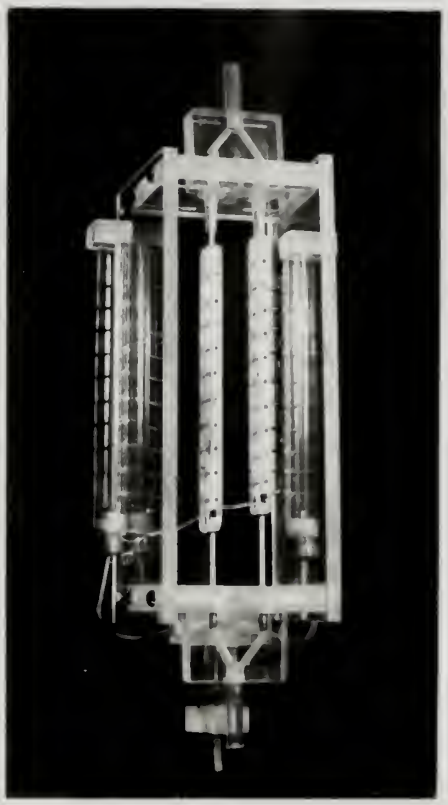

20-NOZZLE CHARGED
AEROSOL UNIT

Figure 5.

C. Electrical Equivalent Circuit

Ideally, the input terminal characteristic of the charge wave generator should be a "pure" capacitance, all of which is attributable to the fluid between inducer electrodes and aerosol droplets in the process of formation. In this ideal case, input current from the voltage source would equal the output current from the generator.

Infact, there is also capacitance between electrodes and capillary tubes, and between leads. That fraction of input current attributable to this portion of the total admittance, and therefore unproductive of output current, must be considered a system loss.

Minization of the undesirable capacitance will be an important consideration in realization of an over-all system capable of self excitation. There are, therefore, essentially two electrical characteristics of the generator indicative of its performance. These are:

(1) The ratio of current output to total input current $= \eta_i$;

(2) The ratio of current output to voltage input $= \beta$

In the case of the 10nozzle aerosol unit, at a frequency of 100 cps, 40 psi air, and input voltage of 65 v. r. m. s., input current was 1.16 μamps with output current of .75 μamp. This results in a value of $\eta_i$ = 64.5 percent. $\beta$ for this unit

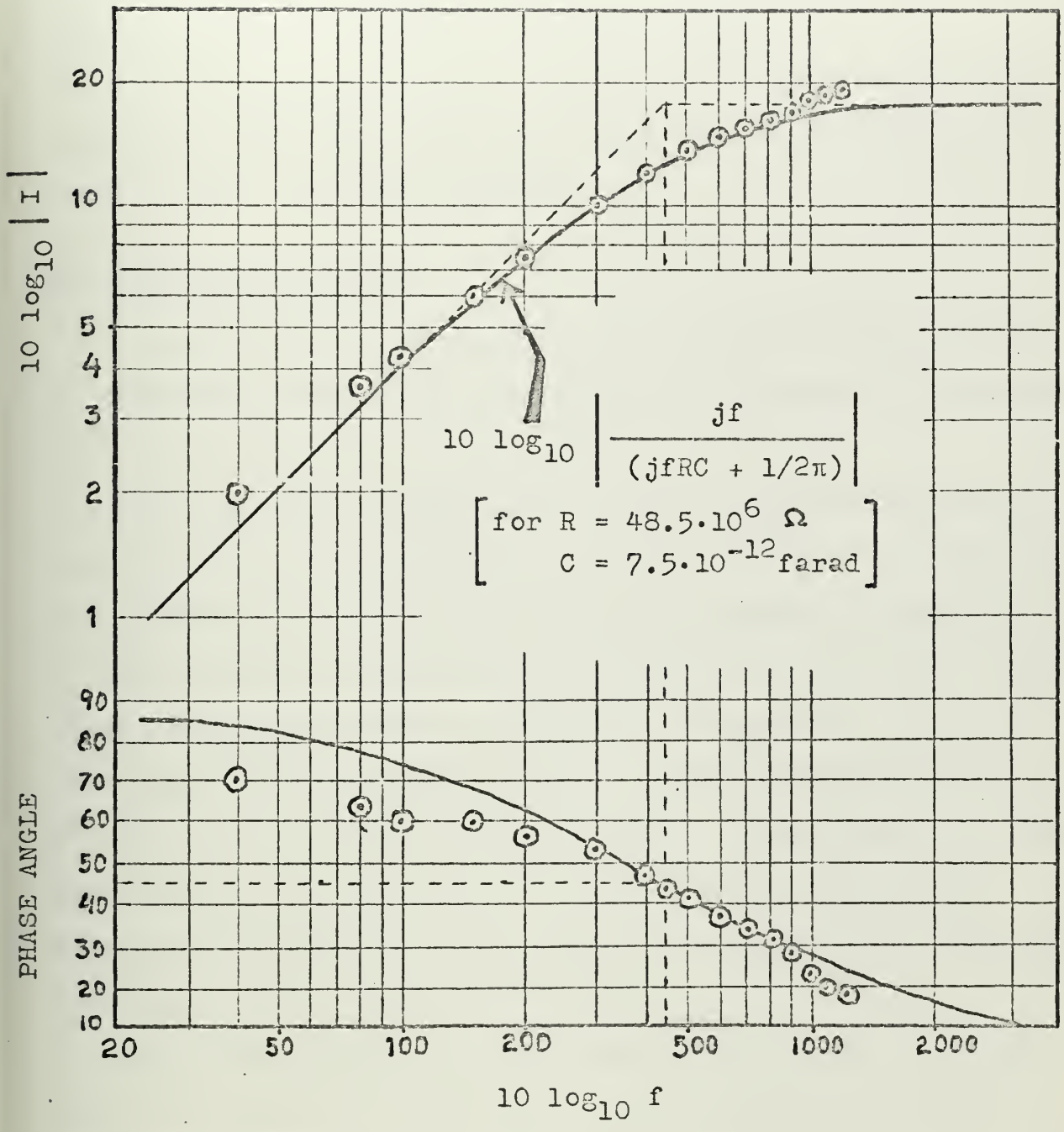


Figure 6. BODE PLOT OF FREQUENCY RESPONSE
for 10-nozzle unit

is equal to the slope of the I vs $V_{in}$ curve in Figure 3. The result is $\beta$ = .012 μamp/volt, where current is measured peak-to-peak and voltage is root-mean square.

Corresponding values for the 20 nozzle unit, using input voltage of 120 v-rms and 20 psi air, were: $\eta_i$ = 1.65/2.5 = 66 percent, and $\beta$ = .014 μamp/volt.

Equivalent Capacitance

Details of the measurements and calculations leading to an estimate of the input capacitance are contained in Appendix C.

Figure 6 shows a "Bode plot" of the frequency response data, summarized in Appendix D. Using the order of magnitude capacitance predicted by the theoretical model of Appendix C, a value of series resistance was selected to place the break-point within the range of available frequencies. For an equivalent length of about 1/2 cm, equation (C.9) predicts a capacitance of about $4 \times 10^{-12}$ farad. Accordingly, a series resistance of 48.5 meg-ohms was used in the measurement apparatus of Figure 18. The equivalent capacitance indicated by Figure 6 is $C = 7.5 \times 10^{-12}$ farad.

Direct calculation of capacitance using equation (C.5) for a frequency of 125 cps and series resistance of 10.2 meg-ohms, yielded a value, $C \approx 6.65 \times 10^{-12}$.

The value which will be taken as the average of these results, for the 10 nozzle unit, is $C = 7 \times 10^{-12}$ farad.

The equivalent model for the complete charged droplet generator will be the simple voltage-controlled current source shown in Figure 7.

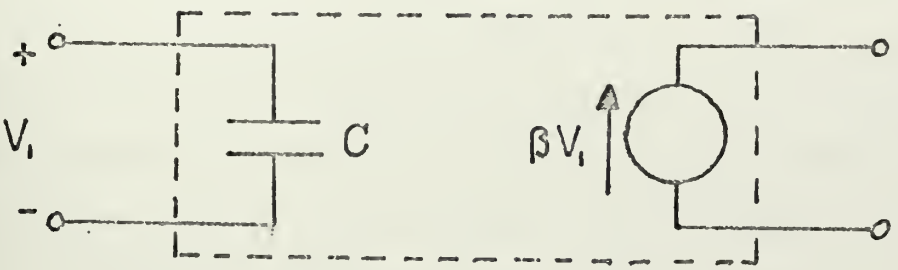


Figure 7. CIRCUIT MODEL FOR CHARGED DROPLET GENERATOR

where $C = 7 \times 10^{-12}$ farad

$\beta = .012$ μa (P-P)/volt (rms)

D. Charge per Droplet and Mobility

From a total of 14 microscope photographs of droplets collected on a castor-oil-coated, 1/16 inch square, length of plexiglass, the most representative was selected for analysis and is shown in Figure 17 in Appendix C. About 6 seconds were required to photograph the droplets after they were collected by being held for about one second, 10 inches from the 10-nozzle aerosol unit, at 40 psi air pressure.

Due to the random nature of the droplet sizes, calculation of the charge distribution must involve rather gross assumptions

as to the most likely mechanism for actual droplet formation and charging.

Droplets were counted and measured over a representative section of Figure 17 comprising 1/8 of the photographed area. The results of the count are contained in table 5., Appendix D.

The calculations outlined in Appendix C were made for each of two different methods of distributing the measured output current with 300 volt (rms) input. From Figure 3, the peak current is about 1.85 μamps, with a flow rate of 1/3 $cm^3$/sec corresponding to 40 psi air pressure from Figure 4b.

Size-dependent Charge Distribution

In order to make allowance for the likelihood of finding more charge on a large droplet than on a small one, average droplet diameter was calculated for three ranges of droplet sizes found in Figure 17. Out of 60 "typical" droplets, the average diameter of the 6 largest was 22.5 μm. the next 15 medium droplets 11.4 μm, and the average diameter of the 39 droplets with diameters less than 10 μm was 5 μm.

On the assumption that charge per drop is distributed in proportion to surface area the following charge per droplet and modified Rayleigh limit comparison results.

(1) Large droplets ($d_1 \approx 22.5$ μm)

$q_1 \approx 8.8 \times 10^6$ electrons/droplet

$q_{max} \approx 3.35 \times 10^6$ electrons/droplet

(2) Medium droplets ($d_m \approx 11.4$ μm)

$q_m \approx 2.28 \times 10^6$ electrons/droplet

$q_{max} \approx 1.21 \times 10^6$ electrons/droplet

(3) Small droplets ($d_s \approx 5$ μm)

$q_s \approx 4.4 \times 10^5$ electrons/droplet

$q_{max} \approx 3.5 \times 10^5$ electrons/ droplet

Numerical Average Droplet Diameter

The usual convention for obtaining average droplet size in an aerosol is

$$d_{avg} = \sum_{n=1}^{N} d_n/N \qquad \text{(III.1)}$$

where N = Total number of droplets in the sample

Applying this definition to the data of Table 5 yields an average diameter

$$d_{avg} \approx 8.25 \text{ μm.}$$

the charge per droplet becomes

$$q_{avg} \approx 10^4 \text{ electrons/droplet}$$

and

$$q_{max} = 7.5 \times 10^5 \text{ electrons/droplet}$$

Mobility

Applying the foregoing results to equation (C.18) yields

an approximate average mobility, K (in units of coul-sec/kg or $\frac{m/sec}{volt/m}$).

(1) Large droplets ($d_l$ = 22.5 μm)

$K = 3.62 \times 10^{-4}$

(2) Medium droplets ($d_m$ = 11.4 μm)

$K = 1.85 \times 10^{-4}$

(3) Small droplets ($d_s$ = 5 μm)

$K = 8.1 \times 10^{-5}$

(4) Numerical average droplets ($d_{avg} \approx$ 8.25 μm)

$K = 1.14 \times 10^{-6}$

E. Effect of Increasing Conductivity of the Water

In view of the high rate of formation of the water droplets and a qualitatively observed fall-off of output current magnitude with increasing frequency, an observation of output current was made before and after a sudden increase in salinity of the water fed to the 10-nozzle aerosol unit.

The apparatus was adjusted for an output current of 1.4 μamp (P-P) with 40 psi air pressure and siphon height of about 20 inches.

A "normal" saline solution (.9 gm. NaCl per 100 cc. $H_2O$) was substituted for the triple-distilled water (used in all other experiments of this report) and the output

current was observed to increase to 2.0 μamp (P-P). The current remained at this level as the system was being flushed with tap water. This experiment was repeated several times with consistent results.

## IV. DISCUSSION OF RESULTS

Due to the extremely complicated nature of the actual interplay between system parameters, as previously discussed, the results must be viewed as more qualitative than quantitative. The original objective was to investigate the synchronous EFD generator and, hopefully, to establish its feasibility as a practical energy conversion system. The results are encouraging in this regard, and are considered demonstrative of the fact that such a system has sufficient potential to more than justify further development.

The fact that the aerosol droplets are formed at a high rate from distilled water did not seriously limit the induced charge per droplet at the relatively low frequencies investigated. The simple instrumentation employed in measuring output current was not adequate for satisfactory determination of the response of the output current to increasing excitation frequency. This was due to the increasing capacitive admittance between the inducer electrodes and collector screen, and decreasing wave length of the charge stream as frequency increased. The former resulted in "noise" pick-up swamping the charged aerosol signal, which was at the same time being reduced by the increasing width of the collector screen relative to the charge wave length.

The 64 - 66 percent output/input current efficiency

achieved by this relatively simple generator design seems highly promising for eventual self-excited operation. It is quite likely that more precise construction and improved electrode design might increase this efficiency to 80 percent or better.

The efficacy of the induction method for charging the aerosol droplets is considered to have been established by these results, at least up to frequencies of a few hundred cps. The field in the inducer section was not carried up to breakdown strength in order to avoid burning that capillary tube furthest off-center in its inducer. A machine-made nozzle array would possess a more uniform gap width and allow larger current output per nozzle. In addition, the output current can be increased by increasing the density of nozzle mountings, so that no further attempt was made to increase aerosol currents beyond those of Figure 3 for the purposes of this report.

Another factor, equally as important as obtaining an increase in aerosol current, is the concurrent increase in droplet density within the channel. Since a practical energy converter will have to retrieve energy from the gas-dynamic flow, a high droplet density is required for effective electrical/mechanical coupling. The very low mobilities attained by these droplets, as described in the previous chapter, will only by useful if such is the case.

In this study the aerosol was injected into a separate

air flow, but one obvious way to increase droplet density in the channel is to use only the air which comes from the charged spray apparatus. This might require changes in channel configuration for multistaging, but such modifications should be minor compared to the increased efficiency that would be realized.

Another advantage of the sprayed aerosol method is the fact that recirculation in a closed system would require no additional energy input. Since aerosol liquid is siphoned to the mixing nozzles, it need only be collected at the downstream end of the system and provided with a return path.

In the previous chapter, two different methods were used in attempting to calculate the charge per aerosol droplet. While the size-dependent breakdown seemed intuitively to be a more accurate representation of the actual situation at the point of droplet formation, the resulting charge per droplet exceeded the modified Rayleigh limit used as an upper extremum.

There are several possible explanations for this, in addition to the obvious conclusion that the assumption itself may be invalid.

(1) The method used to collect and observe the droplets introduced a six second delay between the time of collection and that of photographing the results. For the larger droplets it seems reasonable to assume that

evaporation will just about off-set the flattening out of the droplets in the surface of the castor-oil-coating, and the observed diameter will be a fairly accurate measure of the original spherical diameter. For droplets on the order of 5 microns and smaller, this will undoubtedly not be the case. In fact, it was observed that the lifetime of droplets on the order of one or two microns diameter, even on the castor-oil, was one or two seconds, at most. If a significant number of one to 3 or 4 - micron diameter droplets were lost in this way, it would explain the high calculated droplet charges, since the ratio of surface area to volume is inversely proportional to diameter.

(2) Since the output current was observed to be somewhat conductivity limited, the actual circumstances may be controlled in part by the time it takes for a droplet to be formed. If all droplets are initially formed at the same rate, the result may be a tendency toward a more uniform value of charge per droplet, irrespective of size.

(3) The fact that the charge per droplet calculated on the basis of an average size of 8.25 μm was an order of magnitude below Rayleigh's limit, may indicate that a truer mean value lies somewhere between the two assumptions.

(4) From observation of the spray formation point it is apparent that the liquid emerging from a capillary

tube is immediately drawn radially outward to meet the air jet. It may be that large droplets are formed before contact with the air jet, whereupon they are further atomized. In this event it would not be possible to achieve charge concentrations approaching Rayleigh's limit because of the increase in area to volume ratio through atomization. Here again, the actual mechanism may well be a random intermediate process where portions of the liquid "sheet" are still intact upon reaching the air jet, and therefore some charge induction may take place within the actual atomization process.

The interactions which take place in creating the aerosol spray are too complex to permit resolution of these questions here, but a more detailed investigation of the problem would be worthwhile if eventual optimization is carried out for this type of system.

If there are a large number of very small droplets, as suggested in the foregoing, it would explain a good portion of the signal deterioration with distance down the conversion channel, described in Reference 19. As the droplets evaporate, the charges they carried become highly mobile, and very little loading would be required to pull them out to the channel walls. Since significant loading has not yet been investigated in the conversion channel, the experimental determination of mobility effects in the synchronous system

is recommended as an objective for further study.

By increasing the operating frequency the efficiency of the system should be improved, since either the size of the generator can be decreased while retaining the same number of wave lengths, or more wave lengths can be accommodated and/or flow velocity increased. This would probably introduce no further constraints on the system other than a requirement for increasing the conductivity of the aerosol liquid.

With size dependence a factor in the amount of charge carried per droplet, it can be seen, from the results in Chapter III, that for large aerosol droplets mobility becomes directly proportional to droplet radius. Optimization of the over-all system may involve compromise between increased current flow and maximum coupling with the transport medium. In both cases, an increase in aerosol density is called for, and the optimum droplet size will probably require a saturated transport medium to avoid evaporation in the conversion channel.

## V. CONCLUSIONS AND RECOMMENDATIONS

### A. Conclusions

(1) The synchronous EFD energy conversion process is a feasible method of producing a-c electrical energy from fluid mechanical energy.

(2) It may be more advisable to view the system as advantageous from the standpoints of reliability, light weight, and simplicity, rather than for expectation of high over-all energy conversion efficiency.

(3) Achievement of electrical self-excitation should be feasible with relatively minor improvement in efficiency of the experimental system.

(4) The charge induction method used in this investigation is capable of producing a distortionless sine wave of charged droplets without mechanical or electrical complexity or prohibitive input losses.

(5) The use of distilled water did not impose a serious limitation on the magnitude of induced charge despite the high rate of formation of the aerosol droplets.

(6) The charged droplet generator, as described, does seem to possess adequate potential for the further development

of a practical synchronous EFD system.

(7) The use of charged droplets larger than 50 to 100 microns should probably be confined to ballistic systems.

B. Recommendations

(1) Significant loading of the charged droplet flow in the conversion channel should be investigated in order to better ascertain the nature of mobility effects and system performance capability for a synchronous EFD system.

(2) System development seems to have reached the point where attainment of self-excitation is a feasible next step . This should most likely be attempted with increased nozzle density and elimination of the additional transport medium (flow fan) or the confining of its use to electrode boundary layer control.

(3) Valuable information would result from detailed investigation of the electrical and atomization interactions at the nozzles. The objective would be to determine the actual charge distribution over the range of droplet sizes found in the aerosol, to the eventual end of optimizing the design with respect to mobility and current output.

(4) Experiments should be conducted with synchronous systems operating at higher frequencies and higher conductivity liquids.

(5) More sophisticated instrumentation for measuring aerosol current, especially at higher frequencies, should be developed. Refinement of the method of measuring droplet diameters should also accompany recommendation (3) above.

# VI. APPENDIX

# VI. APPENDIX

## A. Theoretical Background

### 1. Theory of the General Synchronous Interaction

To aid in analysis the model would be simplified to an effective thin stream of charge as in Figure 8.

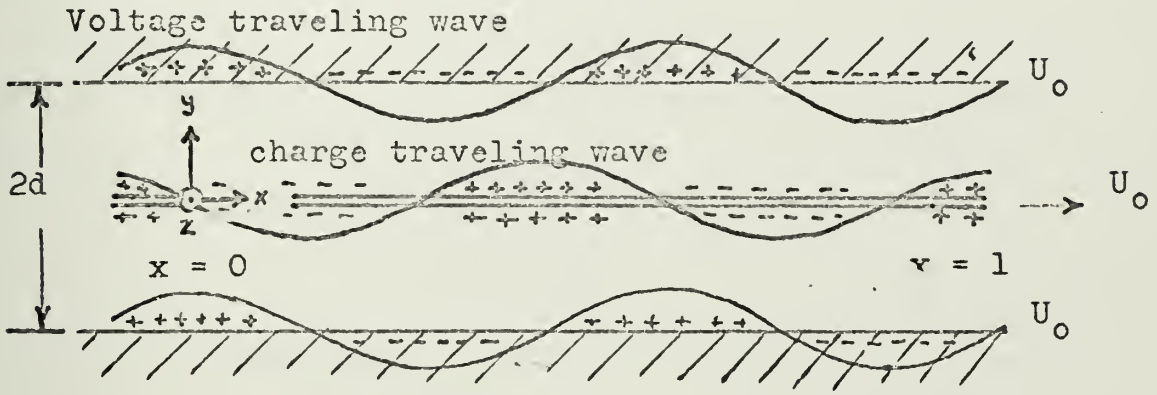


Figure 8.

THEORETICAL MODEL for GENERAL SYNCHRONOUS INTERACTION

The space between the charge wave and the channel walls is analagous to the air gap in a rotating electromagnetic synchronous machine. Just as the leading or lagging phase relationship between rotor and stator determines the direction and magnitude of energy transfer in the rotating machine, the same phase relationship exists between the traveling electric fields in the alternating EFD generator. This is intuitively apparent from Figure 8 and the mathematical analysis presented in the Appendix in Reference 19. A similar analysis of the

theory will be outlined here for the general case as illustration of the interaction mechanism.

The basic equations, in differential form, which must be satisfied within the channel are:

$$\text{Faraday's induction law} \quad \bar{\nabla} \times \bar{E} = 0 \tag{A.1}$$

$$\text{Gauss' Law} \quad \bar{\nabla} \cdot \varepsilon_o \bar{E} = \rho = 0 \tag{A.2}$$

These readily lead to the definition of a scalar potential which must satisfy LaPlaces equation between the channel walls.

$$\varphi \equiv -\bar{E} \tag{A.3}$$

whereupon:

$$\nabla^2 \varphi = 0 \tag{A.4}$$

It is further assumed that the system can be considered semi-infinite in the Z-axis direction and that spacial derivatives with respect to Z are equal to zero. For simplicity, the symmetry of the problem will be used to justify solving the problem only in the upper half of the channel. The sinusoidal nature of the component waves will be observed by defining the charge and voltage waves as:

$$\sigma = \mathrm{Re}[\hat{\sigma}_o e^{j(\omega t - kx)}]$$

and (A.5)

$$\varphi = \mathrm{Re}[\hat{\varphi}(y) e^{j(\omega t - kx)}]$$

Since the system is assumed synchronous, the relationship

$$U_o = \frac{\omega}{k} \tag{A.6}$$

must be true. Solving LaPlace's equation leads to

$$\hat{\varphi}(y) = \hat{A} \sinh ky + \hat{B} \cosh ky \tag{A.7}$$

The boundary condition at the wall (y = d) requires that:

$$\hat{V}_o = \hat{A} \sinh kd + \hat{B} \cosh kd \tag{A.8}$$

The other boundary condition arises from applying Gauss' integral law to the upper half of the charge sheet at y = x = 0. That is:

$$\oiint_A \varepsilon_o \bar{E} \cdot da = \iiint_V \rho_o \, dv = \iint_A \frac{\sigma_o}{2} \, da \tag{A.9}$$

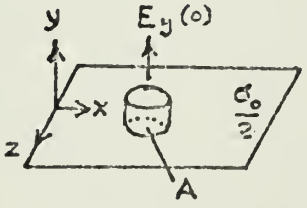


Figure 9. Gaussian "Pillbox" at charge sheet

By symmetry with the other half of the channel, the only contribution to the closed surface integral is $A\varepsilon_o E_y(0)$ and, therefore:

$$\hat{E}_y(y=0) = \frac{\hat{\sigma}_o}{2\varepsilon_o} = -\left.\frac{\delta\varphi}{\delta y}\right|_{y=0} \qquad (A.10)$$

It then follows that the other boundary condition requires

$$\hat{A} = -\frac{\hat{\sigma}_o}{2\varepsilon_o k} \qquad (A.11)$$

and, from (A.8):

$$\hat{B} = \frac{\hat{V}_o + \dfrac{\hat{\sigma}_o \sinh kd}{2\, k\varepsilon_o}}{\cosh kd} \qquad (A.12)$$

In analyzing the forces on the charge sheet, use will be made of the Maxwell stress tensor method as described in Appendix 1 in Reference 17.

In this case the tensor at the charge sheet reduces to

$$T = \begin{bmatrix} T_{xx} & T_{xy} & T_{xz} \\ T_{yx} & T_{yy} & T_{yz} \\ T_{zx} & T_{zy} & T_{zz} \end{bmatrix} \qquad (A.13)$$

$$= \left[\begin{array}{ccc} \frac{\varepsilon_o}{2}(E_x^2 - E_y^2) & \varepsilon_o E_x E_y & 0 \\ \varepsilon_o E_x E_y & \frac{\varepsilon_o}{2}(E_y^2 - E_x^2) & 0 \\ 0 & 0 & -\frac{\varepsilon_o}{2}(E_y^2 + E_x^2) \end{array}\right]_{y=0}$$

where $T_{xx}$ represents force per unit area in the x-direction

on a surface normal to that direction, $T_{xy}$ a stress in the x-direction on a surface normal to the y-axis, etc.

The model for the differential section of half of the charge sheet


Figure 10. STRESS TENSOR at CHARGE SHEET

shows that the $T_{xx}$ forces cancel and the resultant stress on half the charge sheet is $T_{xy}$ and the total stress in the x-direction on the charge sheet will be 2 $T_{xy}$. This is the traction in the x-direction, $T_x$.

The symmetry of the model will require cancellation of all forces along the y-axis. However, in the actual system, where the width of the charge sheet is a significant fraction of the channel width, these forces result in detrimental spreading of the charges toward the walls.

In accordance with (A.3),

$$-\bar{E} = \mathrm{Re}\left\{ke^{j(\omega t-kx)}[(-j)(\hat{A}\sinh ky + \hat{B}\cosh ky)(\bar{i}_x) + k(\hat{A}\cosh ky + \hat{B}\sinh ky)(\bar{i}_y)]\right\}$$

or:

$$\equiv \mathrm{Re}\left\{e^{j(\omega t-kx)}[(\bar{i}_x)\hat{E}_x + (\bar{i}_y)\hat{E}_y]\right\} \qquad (A.14)$$

Evaluating y = 0,

$$\hat{E}_x = + jk\hat{B}e^{j(\omega t - kx)}$$

$$\hat{E}_y = - k\hat{A}e^{j(\omega t - kx)} \qquad (A.15)$$

Now, the time average value of the traction becomes

$$\langle \tau_x \rangle = 1/2 \; Re[2\varepsilon_o \hat{E}_x \hat{E}_y^* ] \qquad (A.16)$$

Appropriate substitutions yield

$$\langle \tau_x \rangle = + \frac{k}{2} Re[j\hat{\sigma}_o \left( \frac{\hat{V}_o^*}{\cosh kd} + \frac{\hat{\sigma}_o^* \tanh kd}{2k\varepsilon_o} \right) ]$$

$$= \frac{k}{2 \cosh kd} Re[j\hat{\sigma}_o \hat{V}_o^* ] \qquad (A.17)$$

At this point it becomes possible to readily observe the effect of the phase relationship between the voltage and charge waves.

Rewriting (A. 17) in polar form:

$$\langle \tau_x \rangle = \frac{k\sigma_o V_o}{2 \cosh kd} Re[e^{j(\pi/2 + \phi_c - \phi_v)}] \qquad (A.18)$$

where $\phi_c$ and $\phi_v$ are the phase angles of charge and voltage (at $\omega t - kx = 0$), respectively.

A further change of notation, together with multiplying $\langle \tau_x \rangle$ by $U_o$, results in an expression for time-average power flow per unit area of charge sheet.

$$\left\langle \frac{P_{avg}}{\text{unit area}} \right\rangle = \frac{k\sigma_o V_o U_o}{2 \cosh kd} \cos\left(\frac{\pi}{2} - \delta\right)$$

$$= \frac{k\sigma_o V_o U_o}{2 \cosh kd} \sin\delta \qquad \text{(A.19)}$$

where $\delta \equiv \phi_v - \phi_c$

Taking the charge sheet as reference

$$\delta = \phi_v$$

It is now apparent that when the voltage leads the charge ($\delta>0$) by $90^\circ$, the force on the charge sheet is maximum in the direction of flow and the system acts as a pump. Similarly, when the voltage lags by $90^\circ$, the energy transfer is greatest in retarding the flow and the system becomes a generator with flow dynamic energy of the charge sheet being converted to electrical energy in the walls.

Figure 8 depicts the generating case. A more complete analysis of this case, the various modifications obtainable together with their further implications, and experimental results are to be found in Reference 19, a thesis in preparation

concurrently with this one.

2. Mobility Considerations

The foregoing analysis is dependent on the assumption that the charges are rigidly coupled to the moving sheet. Evaluation of this assumption is extremely pertinent to a gas dynamic system since the coupling is not rigid, but is, infact, dependent on viscous slip forces which oppose the electrical retarding force. In this way the charged droplets interact with the gaseous medium to transfer energy either to or from the flow, as the case may be.

It can now be seen that the amount of slippage required in order to produce the viscous force will be a loss in the net power available from the system, since from equation (A.19) power is proportional to the speed of flow of the charges.

With the slip velocity defined as u, Mobility (K) has traditionally been defined as the ratio of slip velocity to electric field.

$$K \equiv \frac{u}{E} \qquad \text{(A.20)}$$

Another detrimental effect of high mobility, is rapid lateral drift of charged droplets toward the side walls. For a droplet in the exact center of the channel, lateral forces would counterbalance, but obviously this would be an unstable condition even if it were physically attainable.

Since mobility cannot be reduced to zero in a fluid system, lateral drift can, at best, be minimized or compensated, but probably never eliminated.

The mechanics of the interaction of ions and droplets in a fluid dynamic flow are well summarized in several of the references, particularly Reference 7 and Reference 15.

The following is from a more detailed summary found in Reference 15.

Since mobility is largely dependent on particle size, the usual three regions of categorization are by droplet diameter.

(1) Small droplets (a <.002 microns)

These include ions and other particles whose size is comparable to that of an air molecule. Here the coupling forces are predicted by molecular kinetic theory and both measured and theoretical mobilities decrease with increasing pressure. The relationship for mobility derived from Longevin s theory is

$$K = 3/4 \frac{q}{\delta(8\pi P\rho)^{1/2}} (1 + m/M)^{1/2} \qquad (A.21)$$

where $\delta$ = distance of closest approach

$m$ = ionic mass

$M$ = mass of gas molecule

$\rho$ = gas density

$P$ = gas pressure

While this equation predicts mobilities larger than those experimentally measured, the mobilities of ions are too large in gaseous media for adequate EFD efficiency.

(2) Intermediate droplets (.002 < a < .5 micron)

Here a compromise between kinetic theory and viscous coupling is usually considered. The equation listed in both References 7 and 15, and derived from the Stoke-Cunningham law, is

$$K = \frac{q}{6\pi\mu a}\left(1 + \frac{L}{A}\right) \qquad (A.22)$$

where L = mean free path

A = experimentally measured constant (on the order of .8)

There have been correction factors added to the second term for the larger values of L/A, but the equation as it stands is indicative of the tendency toward the Stokes law mobilities as droplet size increases.

(3) Large droplets (a>.5 μm)

For large droplets Stokes law leads to the simple expression for mobility,

$$K = \frac{q}{6\,\pi\,\mu\,a} \qquad (A.23)$$

For given charge per droplet it is evident that mobility can be decreased by increasing the size of the droplets. As previously mentioned, however, in the case of the induction system presented here the charge per droplet is also size dependent, as is the moisture accumulation on the channel walls.

3. Theoretical Limit on General EFD Process with Slip

A simple model of a direct EFD conversion section is shown in Figure 11. Irregardless of the actual interactions which may take place within the section, use of Maxwell stress tensor analysis provides a convenient method of discerning the maximum energy conversion which could be realized.

Several simplifying assumptions will be made, both for the sake of aiding analysis, and since they clearly provide a limiting case.

(1) The electric field components in the x-axis direction are uniform across a constant area channel cross-section.

(2) Energy changes in the fluid transport medium will be expressed as an equivalent pressure drop at constant flow velocity, $U_o$.

(3) Flow frictional losses at walls and channel

ends will be neglected.

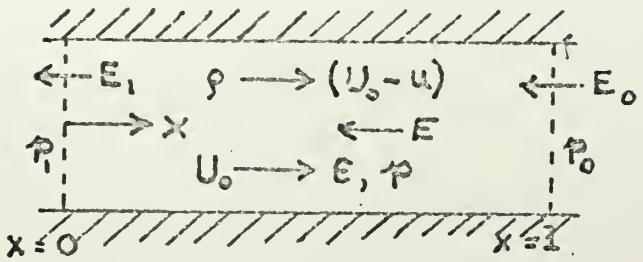


Figure 11. GENERAL d-c EFD CONVERSION SECTION MODEL

Whether the channel is rectangular or cylindrical, stress components integrated over the side walls will cancel. The electrical stress magnitude on the channel section will be the difference between those on the surfaces normal to the x-axis.

$$\tau_x = \frac{\varepsilon}{2} E_1^2 - \frac{\varepsilon}{2} E_o^2 \qquad (A.24)$$

Equilibrium for the section requires the electrical stress and flow pressure differential to balance.

$$\frac{\varepsilon}{2} (E_1^2 - E_o^2) = p_1 - p_o \equiv \Delta p \qquad (A.25)$$

This expression will be maximum for $E_o = 0$, and $E_1$ at field breakdown strength, $E_b$.

$$\Delta p_{max} = \frac{\varepsilon}{2} E_b^2 \qquad (A.26)$$

The fluid dynamic power per unit area delivered to the conversion section will be

$$\Delta p_{max} \cdot U_o = \frac{\varepsilon}{2} E_b^2 U_o \qquad (A.26)$$

while the electrical power density allowing for significant mobility of the charge carriers will be

$$L_e = \frac{\varepsilon}{2} E_b^2 (U_o - u_1) \qquad (A.27)$$

where $L_e$ is the density of electrical power produced in the section and $u_1$ is slip velocity at the inlet

Substituting equation (A.20) into (A.27)

$$L_e = \frac{\varepsilon}{2} E_b^2 (U_o - KE_b) \qquad (A.28)$$

where K would be a measurable mobility according to the methods of the previous section.

These results are obtained by Lawson[13] in a way which demonstrates internal interaction of the system parameters, but the limiting case result is sufficient here to indicate the field strength limitation and effect of mobility in deterioration of efficiency.

B. Design of the a-c Charged Droplet Source

1. Theoretical Aspects

Corona discharge

The most satisfactory method, to date, for generating charged particles in direct current EFD generators, has been by condensation around, or direct convection of, ions formed from corona discharge at the entrance to the converter. The usual configuration provides an attractor electrode just downstream from a grounded needle (or needles). The field between attractor and needle must be less than breakdown ($E_b$), but sufficiently high to produce a space charge in the vicinity of the corona needle which is picked up by the working medium and carried past the attractor. Since most, if not all, of the ions are not allowed to migrate to the attractor, the energy required to produce this current must be supplied by the medium. Figure 12 is from Reference 14 and shows the general arrangement of one type of corona configuration.

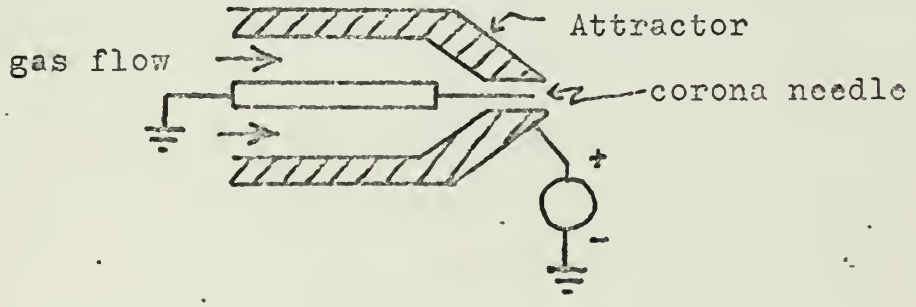


Figure 12. A CORONA DISCHARGE CONFIGURATION

Lawson[14] derives a theoretical relation for the magnitude of the current produced in a corona device which he then modifies to agree with experimental data. He begins by assuming a cylindrical space charge around the needle of radius $R_a$, and constant charge density $\rho_e$. The additional assumption is made that the transport velocity $V_e$ is equal to half the flow velocity V. The current is then approximated,

$$I = \rho_e V \pi R_a^2 \tag{B.1}$$

and the field in the charge cloud ($E_o$) becomes

$$E_o = \frac{\rho_e R_a}{2\varepsilon_o} \tag{B.2}$$

This, together with the definition of mobility, equation (A.21), yields

$$I = \frac{\varepsilon_o V^2 \pi R_a}{K} \tag{B.3}$$

Lawson obtained satisfactory agreement with experimentally obtained currents by including a factor of 30 percent.

$$I = (.3)\frac{\varepsilon_o V^2 \pi R_a}{K} \tag{B.4}$$

Substitution of suitable values corresponding to ions with V = 302 m/sec, $R_a$ = 1.59 mm, at an operating pressure of

19.4 atmospheres, yielded a value of I equal to 120 μa.

In turning his attention to colloidal charge carriers, Lawson assumed slip to be negligible ($V_e = V$) and E was therefore allowed to approach breakdown, $E_b$. Using the same conditions as before, and dividing the resulting expression for $I_{colloid}$ by that for $I_{ion}$, Lawson obtains the ratio,

$$\frac{I_{col}}{I_{ion}} = 1080 / V \qquad (B.5)$$

where V is expressed in m/sec

His experimental values were found to be in general agreement and colloid currents more than adequate for a generator contemplated under the limitations imposed by space charge effects within the channel[12, 13].

Some kind of modified corona method may eventually prove feasible for alternating polarity ion generation, but at the state of present technology, the much lower breakdown potential for positive ions seems to be a prohibitive limitation[14].

Induction method

It was decided, for this investigation, to use capacitive coupling between an inducing electrode and sprayed water droplets to induce charge of opposite polarity on the droplets as they break away. A considerable amount of research has been

conducted in the study of electrical spraying of conducting liquids (References 1, 5, 9, 10, 16) but this has also been with d-c fields and largely for application in thruster design for space vehicles. Droplets formed due to electrical stress instability could be expected to produce a severely non-uniform charge distribution if the signal on the inducing electrode were sinusoidal rather than constant potential. Since the aim of this research was to produce a harmonic free, "clean" sinusoidal charge wave, the instabilities were avoided.

The limiting value of charge that a liquid droplet can support is a well known expression derived by Rayleigh[1]. It is the limiting surface charge density just short of overcoming the surface tension holding the droplet in equilibrium.

The expression for Rayleigh's limiting value of charge on a spherical droplet is

$$q = 8 \pi a^{3/2} \sqrt{\varepsilon_o \gamma} \qquad \text{(B.6)}$$

A similar limiting expression can be readily obtained for the case of a droplet being formed under the combined stresses of electrical field and internal pressure to overcome surface tension. A simple model is shown in Figure 13 which uses the rather gross assumptions of hemispherical shape as the droplet is released, and a uniform electrical field acting

normal to the liquid surface.

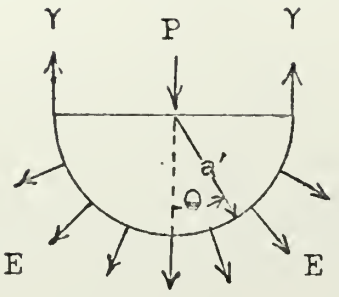


Figure 13. MODEL for MODIFIED RAYLEIGH LIMIT

The electrical stress on the surface is $\frac{E_o}{2} E^2$ and the equation of equilibrium for the hemisphere just prior to separation is

$$\gamma 2\pi a' = \pi(a')^2 P + \int_0^{\pi/2} \frac{\varepsilon_o}{2} E^2 \cos\theta \, 2\pi a \sin\theta (a' \, d\theta)$$

$$= \pi(a')^2 \left[P + \frac{\varepsilon_o E^2}{2}\right] \qquad \text{(B.7)}$$

If the liquid is considered to be a "perfect" conductor, Gauss' law at the surface of the drop requires that electrical displacement ($\varepsilon_o E$) be equal to the surface charge density ($\sigma$). Equation (B.7) becomes,

$$2\gamma = a' \left[P + \frac{\sigma^2}{2\varepsilon_o}\right]$$

$$= a' \left[P + \frac{(q/2\pi a'^2)^2}{2\varepsilon_o}\right] \qquad \text{(B.8)}$$

After separation the droplet radius, a, is obtained by equating the hemispherical volume to that of the spheroid, whence

$$a' = a.2^{1/3} \tag{B.9}$$

Substituting (B.9) into (B.8) and solving for the charge per droplet

$$q = 4\pi\sqrt{2}\sqrt{\varepsilon_o}\, a^{3/2}\sqrt{\gamma - \frac{P.a}{2^{2/3}}} \tag{B.10}$$

It can be seen that for this model, if the pressure differential is neglected, the maximum charge per droplet becomes approximately 70 percent of Rayleigh's limiting value. While this model could not be expected to accurately represent the complex situation of the aerosol spray, equation (B.10) will be used as a basis for comparison since it would undoubtedly provide an upper limit.

2. Aerosol Generator Design

The two nozzle designs are similar enough that only the 20-nozzle unit will be described in entirety. The electrode configuration of the "fine droplet" unit is shown in Figure 16.

Figure 14 is a schematic of the over-all configuration of the charged aerosol generator. The major elements are the compressed air harness, the water siphon line and nozzle

supply headers, and the two 5-nozzle spray units.

The channel section formed by the generator unit is 3 inches long and tapered in order to adapt the flow fan section to the main conversion channel, and to provide some convergence of the air flow as it picks up the aerosol. The entrance cross-sectional dimensions are 6 inches by 2-3/4 inches and the exit dimensions are 6 inches by 2-1/4 inches to match those of the downstream conversion section.

The general simplicity of the design is perhaps best illustrated by the fact that all parts except tubing were constructed of plexiglass, with a drill press being the only power tool required.

Figure 15 shows the detailed construction parameters of the 20-nozzle aerosol unit. As previously observed, the peculiarities of the over-all system provided the majority of the design constraints. The only basic requirements of the aerosol generator itself are the positioning of a water carrying capillary tube in the center of the cylindrical, high velocity air jet, and the arrangement of the charge inducing electrode in close proximity to the mixing point.

To produce a uniformly fine spray, the water must be siphoned to the nozzle by the concentric air jet. In general, the greater the siphon distance the finer the spray. The siphon height for the charged aerosol generator also has a small effect on the current output, since the flow rate is

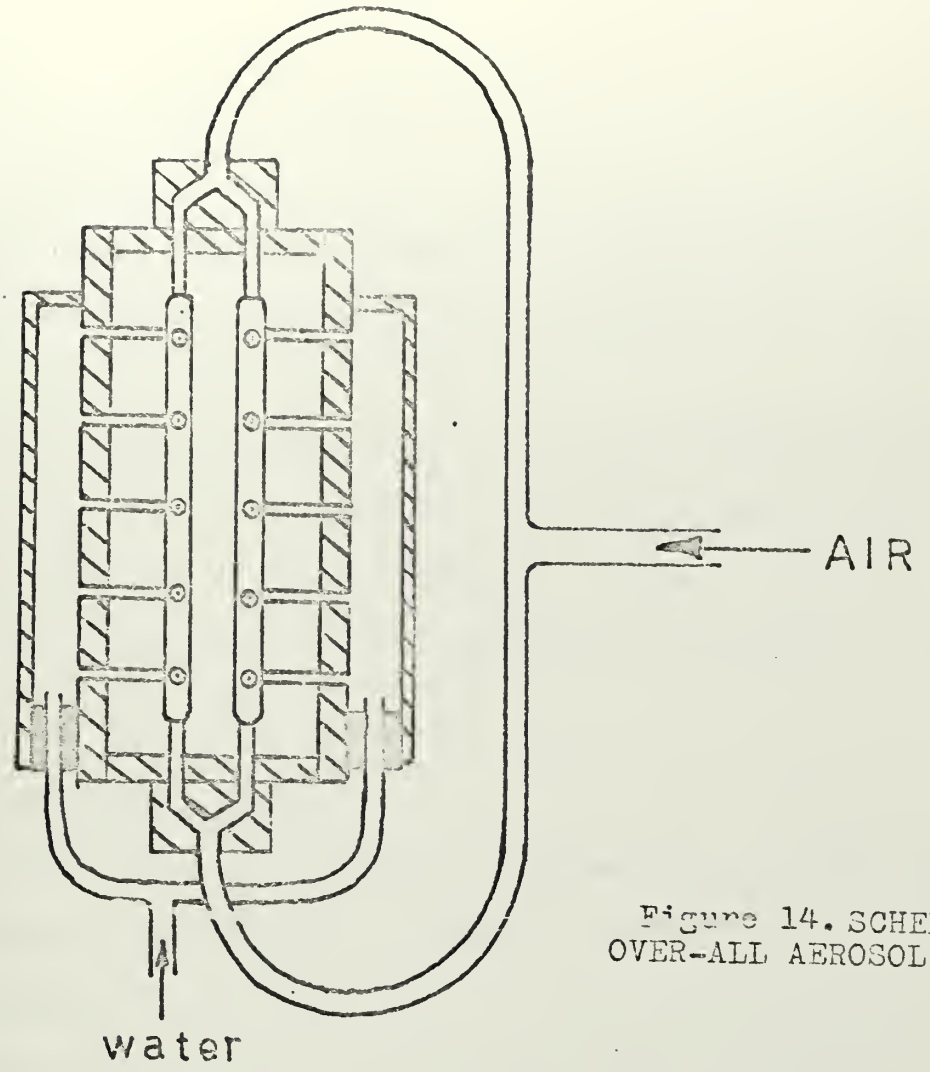


Figure 14. SCHEMATIC of OVER-ALL AEROSOL GENERATOR

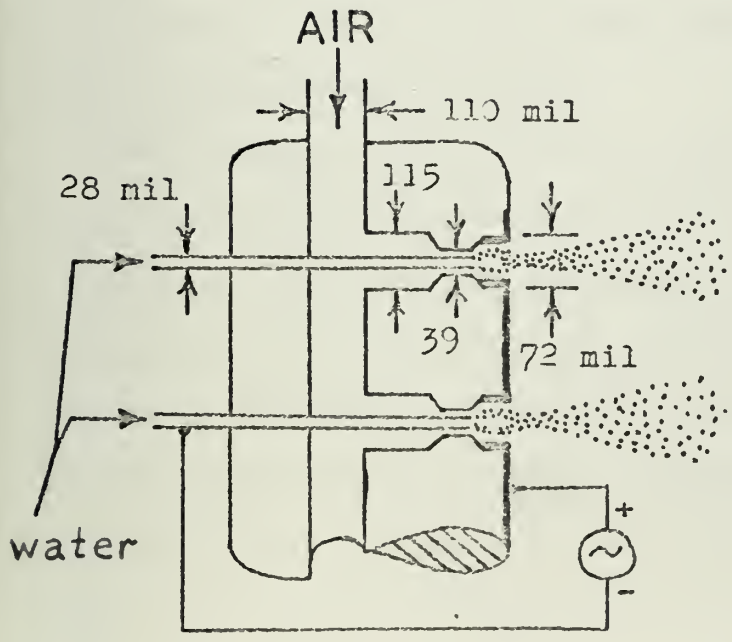


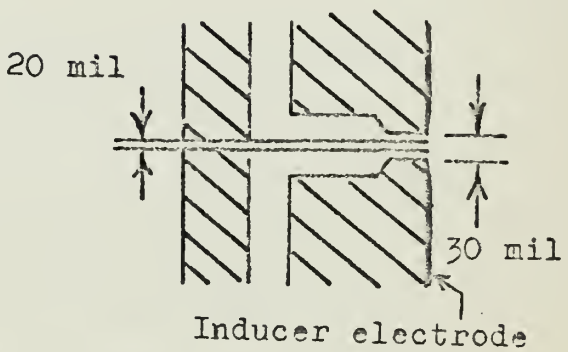


Figure 16.
CONFIGURATION of 10-NOZZLE INDUCER

Figure 15. SCHEMATIC of 20-NOZZLE UNIT

greatest for small siphon distances. A siphon height of about 23 inches seemed to be the best compromise for this system.

The size of the air feed channel in the nozzle assembly has to be large enough to ensure a reasonably uniform air pressure feeding all of the individual nozzles. This was especially true with the limited laboratory compressed air supply.

3. Measuring Droplet Size

In order to calculate the average charge per droplet and charge-to-mass ratio for the traveling wave particles, it is necessary to know the average size of the aerosol droplets. Probably the simplest way to accomplish this, in theory, is to collect the droplets on a slide and photograph them under a microscope. This is the method that was used in obtaining the data for this thesis report.

When highly accurate results are required, the process of collecting the droplets becomes critical. Under such conditions, the aerosol is usually allowed to fill a saturated container and a very slender collecting glass is passed carefully through the fog at an accurately controlled rate. If the collector presents an excessively large cross-section in the direction of motion the smaller droplets are swept aside and only the larger ones penetrate the boundary layer to strike the slide.

Another problem which must be faced, irregardless of the accuracy required, is the short lifetime of micron sized droplets in "dry" air. In order to prevent rapid evaporation the slide is coated with castor oil which has been in contact with water long enough to have become saturated.

In view of the fact that the aerosol is injected into a dry air stream when used in the present synchronous system, the droplets were collected in the dry air environment on the coated slide and the results are considered more or less representative of the conditions as the aerosol enters the converter section. Since the droplets require only 1/20 sec. to traverse the channel, it was assumed that further evaporation within the conversion section could be neglected. Figure 17 shows a typical microscopic view of the collected droplets at about 330 X.

## C. Calculations

### 1. Electrical Capacitance of Aerosol Generator

The electrical circuit model of the apparatus used to measure the equivalent capacitance is shown in Figure 18, where $V_s$ was a variable frequency (10 - 1200 cps) sinusoidal voltage source. $V_1$ and $V_2$ were fed to a dual trace oscilloscope.

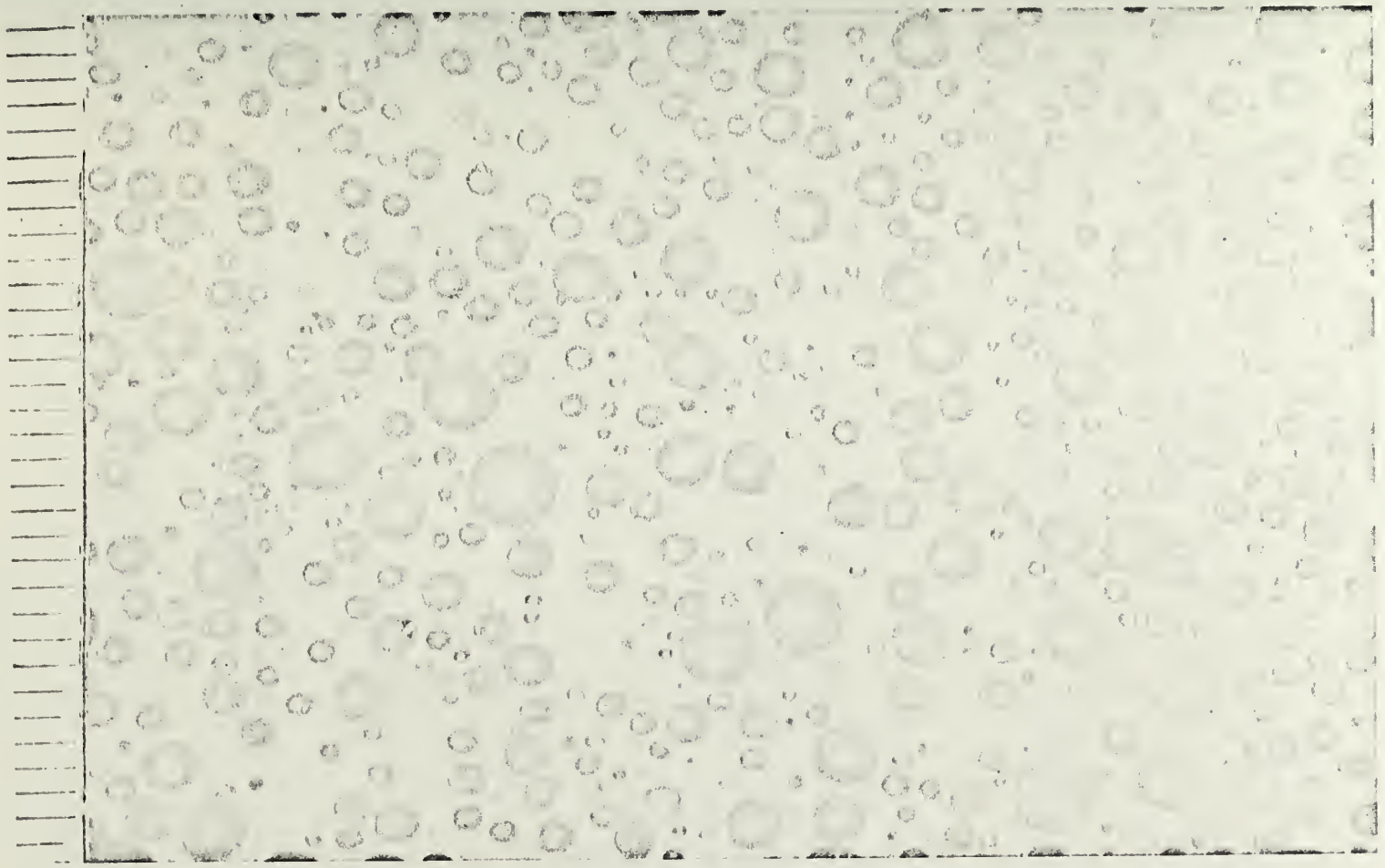

Figure 17. MICROSCOPE PHOTOGRAPH OF COLLECTED AEROSOL

(scale divisions at left are 10 microns apart)

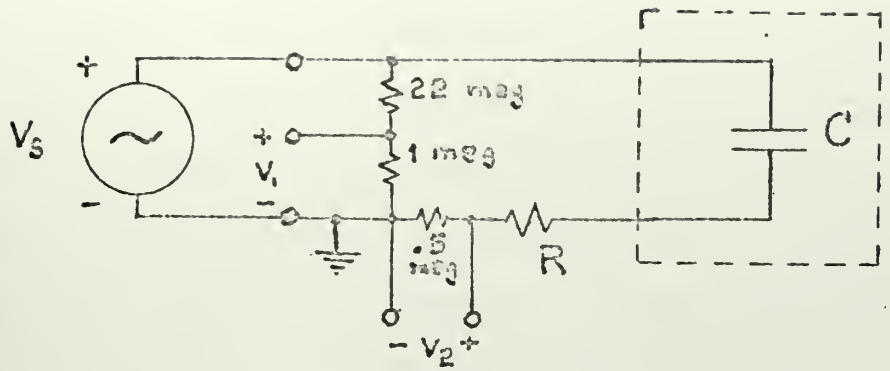


Figure 18. CIRCUIT MODEL of INPUT TEST APPARATUS

Frequency Response

In order to construct a "Bode diagram" with its break-point within the available frequency range, R was set a 48 megohms. In LaPlace transform notation, the admittance relation $I/V_s$ is

$$\frac{I}{V_s} = \frac{2 \cdot 10^{-6} V_2}{23\ V_1} = \frac{Cs}{RCs + 1} \qquad (C.1)$$

In terms of magnitude alone for $s = j\omega$,

$$|I| = |V_s| \frac{\omega C}{[R^2C^2\omega^2 + 1]^{1/2}} \qquad (C.2)$$

taking the logarithm of both sides and multiplying by 10,

$$10 \log_{10} |I| = \text{Constant} + 10 \log_{10}\omega - 5\log_{10}[(RC\omega)^2 + 1] \qquad (C.3)$$

The constant can be ignored in analyzing the data, while the remaining two terms should provide two asymptotic regions. At very low frequencies a plot of 10 $\log_{10}|I|$ vs. 10 $\log_{10}\omega$ should approach a straight line of slope 10 decilogs per decade of frequency. As $RC\omega$ approaches 1 the curve should begin to "break", and at higher frequencies approach a constant value. This can be seen from the limit of equation (C.2) as $\omega$ goes to infinity.

The phase plot of current lead angle vs. 10 $\log_{10}\omega$ provides an additional check on the preceding, because the break point at $RC\omega = 1$ also means a 45 degree phase angle for the denominator term of equation (C.1). The results are plotted in Figure 6 and the data summary is contained in Appendix D.

Numerical Check

Equation (C.2) was used to directly compute the value of capacitance (C) for several values of resistance (R) at a constant frequency (f) of 125 cps.

Letting $R' = (R + .5)$ meg-ohms, and rewriting equation (C.2),

$$\frac{2\,V_2}{23\,V_1 \cdot 10^6} = \frac{C2\pi f}{[(R'C2\pi f)^2 + 1]^{1/2}} \qquad (C.4)$$

then

$$C = \frac{1.59 \cdot 10^{-9}}{\left(\frac{f}{100}\right)\sqrt{\left(\frac{11.5V_1}{V_2}\right)^2 - \left(\frac{R'}{10^6}\right)^2}} \qquad (C.5)$$

Substituting f = 125 cps and holding $V_1$ constant at 10 volts

$$C = \frac{(12.7)V_2 \cdot 10^{-12}}{\sqrt{(1.15)^2 - \left(\frac{V_2}{100} \cdot \frac{R'}{10^6}\right)^2}} \qquad (C.6)$$

With $R' = 10.2 \times 10^6$, the measured value of $V_2$ was .62 volts. Then,

$$C \approx \frac{7.88 \cdot 10^{-12}}{1.15}$$

or

$$C \approx 6.85 \cdot 10^{-12} \text{ farad}$$

Theoretical Model Capacitance

As an order of magnitude check on the measured capacitances, a crude model was calculated. The capacitance between an individual nozzle and its electrode was compared to a cylindrical capacitance of similar dimensions neglecting

fringing, as shown in Figure 19 below.

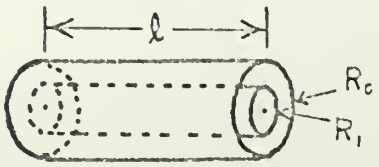


Figure 19. CYLINDRICAL CAPACITANCE MODEL

From the fact that the field in cylindrical coordinates is inversely proportional to radius and from application of boundary conditions at $r = R_1$ and $R_o$, it readily follows that,

$$C = \frac{\varepsilon_o 2\pi l}{\ln(R_o/R_1)} \qquad (C.7)$$

For both nozzle assemblies the ratio $R_o/R_1$ is approximately 2. Substituting numerical values into (C.7)

$$C' = \frac{(1/36\pi)\cdot 10^{-9}(f/m)\cdot 2\pi l(m)}{\ln 2}$$

$$\approx (.8)10^{-12} l(cm) \text{ farad} \qquad (C.8)$$

where $C'$ is the capacitance of an individual nozzle

For the 10-nozzle unit the order of magnitude of capacitance will be

$$C \approx 8\cdot 10^{-12} l(cm) \text{ farad} \qquad (C.9)$$

2. Calculation of Charge per Droplet

"Modified" Rayleigh's Limit

As a further refinement of the base of comparison represented by equation (B.10), a minimum value of pressure (P) (after allowing for a siphon height of 2 feet) will be presumed. For an air inlet pressure to the 10-unit nozzle of 40 psi., siphon height in excess of 23 inches was observed to be at least 1/14 atmosphere, or $73.05 \times 10^3$ dyne/ $cm^2$ pressure. For simplicity of calculation in equation (B.10) therefore, this will be used as reference pressure.

Substituting the appropriate constants into equation (B.10)

$$q_{max} = 4\sqrt{2}\pi a^{3/2} \frac{\left(73.05 \cdot 10^{-9}_{f/m}\right)^{1/2}}{\sqrt{36\pi}} \sqrt{1 - \frac{10^3 \cdot a}{2^{2/3}}}$$

$$= \frac{2}{3}\sqrt{2}\pi a^{3/2} \frac{\left(73.05 \cdot 10^{-13}\ coul^2\right)^{1/2}}{\sqrt{\pi (n \cdot cm^2)}} \cdot \sqrt{10^{-5} \frac{n}{cm} - (.63)10^{-2} \cdot a \frac{n}{cm}}$$

$$= (14.2)10^{-9} a^{3/2} \sqrt{1 - 630a}$$

where "a" is droplet radius in centimeters

Expressing "a" in microns ($10^{-4}$ cm), the expression becomes:

$$q_{max} = (14.2)10^{-15}\, a^{3/2} \sqrt{1 - .63\left(\frac{a}{10}\right)} \qquad (C.11)$$

Equation (C.11) represents the extreme upper limit from Appendix B (P= 0) by neglecting the negative term under the square root, or could be adapted to other pressures by multiplying that term by 13.9 P, where P is expressed in standard atmospheres.

Droplet Flow Rate

The measured flow rates were in terms of $cm^3/sec$ which can be converted to gallons/hour through the conversion factor

$$Q(GPH) = Q(cm^3/sec)\cdot(.95) \qquad (C12)$$

Calculation of Charge per Droplet

In analyzing "fog" droplet data, usual practice is to count droplets by size and use a straight numerical average as the mean droplet diameter. On that basis the data taken from Figure 17 results in an average value of

$$\frac{135 + 171 + 189}{60} = 8.25\ \mu m$$

For the purposes of calculating charge per droplet, this is not necessarily the most meaningful type of average. In order to investigate a size dependent measure of the

charge per droplet, the distribution will be calculated on the basis of average "large droplet", "medium droplet", and average "small droplet".

The average large droplet diameter is $\equiv d_l = \frac{135}{6} \approx 22.5$ μm, the average medium diameter $\equiv d_m = \frac{171}{15} \approx 11.4$ μm, and the average small droplet diameter $\equiv d_s = \frac{189}{39} \approx 5$ μm. The total number of droplets per sec. for a given flow rate is defined,

$$N \equiv (6 + 15 + 39)x = \frac{Q}{\frac{\pi}{6}(6d_l^3 + 15d_m^3 + 39d_s^3)} \qquad (C.13)$$

Using the flow rate for the 10-nozzle unit with air pressure of 40 psi, from Figure 4.

$$Q = \frac{1}{3} \text{ cm}^3/\text{sec} = \frac{10^{12}}{3} (\mu\text{m})^3/\text{sec}$$

Equation (C.13) yields

$$x = \frac{6 \cdot 10^{12}}{60(3)\pi[6(22.5)^3 + 15(11.4)^3 + 39(5)^3]}$$

$$= 1.11 \cdot 10^5 \text{ (60-droplet units/sec)}$$

Since the current per droplet will be roughly proportional to surface area, the output current must be apportioned between the 3 droplet classes according to their respective

fraction of total surface area.

$$\text{Total surface area} \equiv A = \pi x[6d_l^2 + 15d_m^2 + 39d_s^2] \qquad (C.14)$$

For the case in point,

$$A = 5965 \cdot \pi x \quad (\mu m^2)$$

Large droplet fraction $\equiv f_l$

$$f_l = \frac{6d_l^2}{5965} \qquad (C.15)$$

$$= .509$$

The medium droplet fraction is

$$f_m = \frac{1950}{5965} = .327$$

and the small droplet fraction becomes

$$f_s = .164$$

From Figure 3, the output current for a 300 volt input with the 10-nozzle unit, is $I_o$ = 1.85 μa, peak value.

Large Droplet Charge

The fraction of output current carried by large droplets,

$$\therefore I_{ol} = 1.85 \cdot 10^{-6} \frac{\text{coul}}{\text{sec}} (.509) = (.94) 10^{-6} \frac{\text{coul}}{\text{sec}}$$

The charge per droplet becomes

$$q_l = \frac{I_{ol} \text{ coul/sec}}{6 \text{ x droplets/sec}} \qquad \text{(C.16)}$$

$$= 1.41 \cdot 10^{-12} \text{ coul/droplet}$$

Since the electronic unit of charge is $e = 1.602 \cdot 10^{-19}$ coul, the approximate number of electrons per "large" droplet is

$$\frac{q_l}{e} \approx 8.8 \cdot 10^6 \text{ (electrons/droplet)}$$

Medium Droplet Charge

$$I_{om} = .606 \cdot 10^{-6} \text{ coul/sec}$$

and equation (C.16) becomes

$$q_m = \frac{I_{om}}{15 \text{ x}} = 3.65 \cdot 10^{-13} \text{ coul/droplet}$$

and

$$\frac{q_m}{e} \approx 2.28 \cdot 10^6 \text{ electrons/droplet}$$

Small Droplet Charge

$$I_{os} = .304 \cdot 10^{-6} \text{ coul/sec}$$

$$q_s = \frac{I_{os}}{39\ x} = 7.03 \cdot 10^{-14} \text{ coul/droplet}$$

and

$$q_s \approx 4.4 \cdot 10^{5} \text{ electron/droplet}$$

"Modified" Rayleigh Limit

Using equation (C.11), and neglecting the pressure term:

(1) Large droplets

$$q_{max} \approx 14.2 \cdot 10^{-15} (11.25)^{3/2}$$

$$= 5.37 \cdot 10^{-13} \text{ coul/droplet}$$

$$= 3.35 \cdot 10^{6} \text{ electrons/droplet}$$

(2) Medium droplets

$$q_{max} \approx 14.2 \cdot 10^{-15} (5.7)^{3/2}$$

$$\approx 1.94 \cdot 10^{-13} \text{ coul/droplet}$$

$$= 1.21 \cdot 10^{6} \text{ electrons/droplet}$$

(3) Small droplets

$$q_{max} \approx 14.2 \cdot 10^{-15} (2.5)^{3/2}$$

$$= 5.62 \cdot 10^{-14} \text{ coul/droplet}$$

$$= 3.5 \cdot 10^{5} \text{ electrons/droplet}$$

(4) Numerical "Average" Droplets

$$q_{max} \approx 14.2 \cdot 10^{-15} (4.13)^{3/2}$$

$$\approx 1.2 \cdot 10^{-13} \text{ coul/droplet}$$

$$= 7.5 \cdot 10^{5} \text{ electrons/droplet}$$

Charge per Droplet for Numerical "Average" Droplets

Droplet flow rate can be expressed:

$$Q_d(\text{droplets/sec}) = \frac{10^{12} Q}{\frac{4\pi}{3} a^3} \qquad (C.17)$$

$$= \frac{10^{12}(1/3)}{\frac{4\pi}{3} (4.13)^3}$$

$$= 1.13 \cdot 10^{9} \text{ droplets/sec}$$

charge per drop becomes,

$$q_{avg} = \frac{1.85 \cdot 10^{-6} \text{ coul/sec}}{1.13 \cdot 10^{9} \text{ droplets/sec}}$$

$$\approx 1.63 \cdot 10^{-15} \text{ coul/droplet}$$

$$\approx 10^{4} \text{ electron/droplet}$$

Mobility

Substituting numerical values into equation (A.25)

$$K = \frac{2q(\text{coul})}{d(\mu m)} \left(\frac{1}{6\pi}\right) \frac{}{184 \cdot 10^{-6} \frac{gm}{sec\ cm} \cdot 10^{-4} \frac{cm}{\mu m} \cdot 10^{-3} \frac{Kg}{gm}}$$

$$= \frac{q\ (coul)}{d\ (\mu m)}\ 5.77 \cdot 10^{9} \qquad (C.18)$$

D. Summary of Data

TABLE 1.

Single Commercial Nozzle

| $V_i$ (Rms) | Air Press (psi) | Siphon Height | Flow Rate (GPH) | $I_o$ (ua, P-P) |
|---|---|---|---|---|
| 100 | 47 | 24 | .27 | .13 |
| 150 | 52 | 24 | .28 | .19 |
| 200 | 51 | 24 | .28 | .24 |
| 250 | 50 | 24 | .28 | .3 |
| 300 | 50 | 24 | .28 | .37 |
| 200 | 75 | 24 | .36 | .28 |
| 200 | 70 | 24 | .34 | .26 |
| 200 | 65 | 24 | .32 | .25 |
| 200 | 60 | 24 | .30 | .25 |

TABLE 2.

10-Unit Nozzle

| $V_1$ | Air Press | 2nd $I_o$ * | Flow Rate (cm³/sec) | $I_o$ |
|---|---|---|---|---|
| 80 | 40 | .75 | | |
| 100 | 40 | 1.25 | | .8 |
| 150 | 40 | 1.75 | .333 | |
| 200 | 40 | 2.5 | | 1.4 |
| 250 | 40 | 3.0 | | |
| 300 | 40 | 3.8 | | |
| 100 | 50 | 1.3 | .358 | .83 |
| 100 | 45 | 1.3 | .37 | .83 |
| 100 | 40 | 1.25 | .333 | .81 |
| 100 | 35 | 1.15 | .233 | |
| 100 | 30 | .9 | .20 | .69 |
| 100 | 25 | .85 | .143 | |
| 100 | 20 | .7 | | .5 |
| 100 | 15 | .44 | | .23 |
| 100 | 55 | | | .81 |
| 100 | 60 | | | .79 |

*(electrode radius reduced by about 1/3)

TABLE 3.

Input Impedance Frequency response for 10-nozzle unit

($V_1$ = 9.4 (P -P) Refer Figure 18)

| Freq (cps) | $V_2$ (P -P) | Phase Angle ($V_2$ leading $V_1$) |
|---|---|---|
| 40 | .2 | 70 |
| 80 | .36 | 63 |
| 100 | .43 | 60 |
| 150 | .60 | 60 |
| 200 | .74 | 57 |
| 300 | 1.00 | 54 |
| 400 | 1.20 | 46 |
| 500 | 1.36 | 42 |
| 600 | 1.44 | 38 |
| 700 | 1.52 | 35 |
| 800 | 1.6 | 32 |
| 900 | 1.68 | 28 |
| 1000 | 1.8 | 23 |
| 1100 | 1.86 | 20 |
| 1200 | 1.9 | 18 |

TABLE 4.

20-Nozzle Unit

| $V_1$ (Rms) | Air Press (psi) | Siphon Height (inches) | $I_o$ ($P_1$ -$P_2$) amp | Flow rate ($cm^3$/sec) |
|---|---|---|---|---|
| 70 | 30 | 23 | .83 | |
| 100 | 30 | 23 | 1.5 | |
| 150 | 30 | 23 | 2.0 | .906 |
| 200 | 30 | 23 | 3.0 | |
| 250 | 30 | 23 | 3.5 | |
| 300 | 30 | 23 | 4.4 | |
| 70 | 25 | 23 | .9 | |
| 100 | 25 | 23 | 1.3 | |
| 150 | 25 | 23 | 2.0 | .834 |
| 200 | 25 | 23 | 2.6 | |
| 250 | 25 | 23 | 3.4 | |
| 300 | 25 | 23 | 4.4 | |
| 70 | 20 | 23 | .83 | |
| 100 | 20 | 23 | 1.2 | |
| 150 | 20 | 23 | 2.0 | |
| 200 | 20 | 23 | 2.4 | .642 |
| 250 | 20 | 23 | 3.4 | |
| 300 | 20 | 23 | 4.2 | |
| 100 | 45 | 23 | 2.0 | |
| 100 | 40 | 23 | 1.9 | |
| 100 | 35 | 23 | 1.6 | |
| 100 | 15 | 23 | 1.0 | .11 |

The photograph in Figure 17 is representative of a number of microscope photographs taken of droplets collected on a 1/16 inch wide strip of plexiglass held for about 1 second 10 inches from the 10-nozzle unit with air pressure of 40 psi and 23 inches siphon height.

Data taken from an average 1/8 section of Figure 17 containing a total of 60 droplets is summarized, and segregated in Table 5.

| | LARGE DROPLETS | | | MEDIUM | | | SMALL DROPLETS | | |
|---|---|---|---|---|---|---|---|---|---|
| | Number | Diameter | Product | Number | Diameter | Product | Number | Diameter | Product |
| | 1 | 30 | 30 | 1 | 15 | 15 | 4 | 2 | 8 |
| | 1 | 25 | 25 | 4 | 13 | 52 | 3 | 3 | 9 |
| | 4 | 20 | 80 | 2 | 12 | 24 | 18 | 4 | 72 |
| | | | | 8 | 10 | 80 | 6 | 6 | 36 |
| | | | | | | | 8 | 8 | 64 |
| TOTAL | 6 | | 135 | 15 | | 171 | 39 | | 189 |



TABLE 5.

Droplet Measurements Taken from Figure 17

## BIBLIOGRAPHY


1. Rayleigh, J.W.S., "On the Equilibrium of Liquid Conducting Masses Charged with Electricity", Phil Mag., 14, 184 (1882)

2. Volrath, R.E., "A High Voltage Direct Current Generator", Physical Review, V42, (298-3-4), Oct. 15 (1932)

3. Stuetzer, O.M., "Ion Transport High Voltage Generators", Review of Sci. Inst., Vol 32-1, 16-22, (Jan 61)

4. Lawson, M.O., Von Ohain, H., Wattendorf, F., "Performance Potentialities of Direct Energy Conversion Processes between Electrostatic and Fluid Dynamic Energy", ARL-178, Aerospace Research Laboratories, Office of Aerospace Research, U.S. Air Force, (December 1961)

5. Hendricks, C.D., Jr., "Charged Droplet Experiments", J. Colloid Sci., 17, 249 (62)

6. Cox, A.L., "Colloidal Electrohydrodynamic Energy Converter", AIAA Journal, 1, 2491-97 (63)

7. Marks, A., Barreto, E., Chu, C.K., "Charged Aerosol Energy Converter", AIAA Journal, 2-1, 45-51 (64)

8. Kahn, B., Gourdine, M.C., "Electrogasdynamic Power Generation", AIAA Journal, 2-8, 1423-27 (64)

9. Hogan, J.J., Carson, et-al, "Factors Influencing Electrically Sprayed Liquids", AIAA Journal, 2, 1460-61 (64)

10. Hendricks, C.D., Carson, R.S., et-all, "Photomicrography of Electrically Sprayed Heavy Particles", AIAA Journal, 3-2, 733-737 (64)

11. Hasinger, S., et-al, "Electro-Fluid Dynamic Energy Conversion Processes for Power Generation", ARL 64-61, Paper Presented at the SIXTH AGARD Combustion and Propulsion Colloquium, Cannes, France, (March 1964)

12. von Ohain, H.J.P., Wattendorf, F., "Potentialities of Direct Electro-Fluid Dynamic Energy Conversion Processes for Power Generation", ARL 64-73, Office of Aerospace Research, U.S. Air Force (October 1964)

13. Lawson, M.O., "Performance Characteristics of Electro-Fluid Dynamic Energy Conversion Processes Employing Viscous Coupling", ARL 64-74, Office of Aerospace Research, U.S. Air Force (October 1964)

14. Lawson, M.O., "Ion Generation by Corona Discharge for Electro-Fluid Dynamic Energy Conversion Processes", ARL 64-76, Office of Aerospace Research, U.S. Air Force, (October 1964)

15. Decaire, J.A., "Effects of Partial Condensation around Ions in Electro-Fluid Dynamic Energy Conversion Processes", S.M. thesis, Wright-Patterson AFB, Ohio: Air Force Institute of Technology, (1964)

16. Hendricks, C.D., Hogan, J.J., "Investigation of the Charge-to-Mass Ratio of Electrically Sprayed Liquid Particles", AIAA Journal, 3-2, 296 (65)

17. Fano, R.M., Chu, L.J., Adler, R.B., Electromagnetic Fields, Energy, and Forces, Second edition, Wiley, New York, 1960.

18. Hasinger, S., "Performance Characteristics of Electro-Ballistic Generators ARL 64-75, Office of Aerospace Research, U.S. Air Force, (October 1964)

19. Reeve, W.F., "Traveling-Wave Synchronous Electrohydrodynamic Power Generation", S.M. Thesis in preparation, Department of EE, Massachusetts Institute of Technology, Massachusetts, (1967)